ARMY RESEARCH LABORATORY

NAFDTD – A Near-field Finite Difference Time Domain Solver

by Traian Dogaru

ARL-TR-6110 **September 2012**

NOTICES

Disclaimers

The findings in this report are not to be construed as an official Department of the Army position unless so designated by other authorized documents.

Citation of manufacturer's or trade names does not constitute an official endorsement or approval of the use thereof.

Destroy this report when it is no longer needed. Do not return it to the originator.

Army Research Laboratory
Adelphi, MD 20783-1197

ARL-TR-6110 **September 2012**

NAFDTD – A Near-field Finite Difference Time Domain Solver

Traian Dogaru
Sensors and Electron Devices Directorate, ARL

REPORT DOCUMENTATION PAGE

Form Approved
OMB No. 0704-0188

1. REPORT DATE *(DD-MM-YYYY)*	2. REPORT TYPE	3. DATES COVERED (From - To)
September 2012	Final	October 2011 to August 2012

4. TITLE AND SUBTITLE
NAFDTD – A Near-field Finite Difference Time Domain Solver

5a. CONTRACT NUMBER

5b. GRANT NUMBER

5c. PROGRAM ELEMENT NUMBER

6. AUTHOR(S)
Traian Dogaru

5d. PROJECT NUMBER

5e. TASK NUMBER

5f. WORK UNIT NUMBER

7. PERFORMING ORGANIZATION NAME(S) AND ADDRESS(ES)
U.S. Army Research Laboratory
ATTN: RDRL-SER-U
2800 Powder Mill Road
Adelphi, MD 20783-1197

8. PERFORMING ORGANIZATION REPORT NUMBER
ARL-TR-6110

9. SPONSORING/MONITORING AGENCY NAME(S) AND ADDRESS(ES)

10. SPONSOR/MONITOR'S ACRONYM(S)

11. SPONSOR/MONITOR'S REPORT NUMBER(S)

12. DISTRIBUTION/AVAILABILITY STATEMENT
Approved for public release; distribution unlimited.

13. SUPPLEMENTARY NOTES

14. ABSTRACT
This report describes NAFDTD, a near-field finite difference time domain software package developed at the U.S. Army Research Laboratory (ARL). This program is based on the finite difference time domain (FDTD) method and is related to the AFDTD software. Unlike AFDTD, which is designed for radar signature analysis in the far field, NAFDTD is an electromagnetic solver for near field geometries. The differences between the two configurations receive particular attention, followed by a presentation of the numerical issues specific to the near field case. The report contains a user's manual for the NAFDTD program, as well as the companion SOURCERECEIVER utility software. Several numerical examples provide software validation.

15. SUBJECT TERMS
Finite difference time domain, computational electromagnetics

16. SECURITY CLASSIFICATION OF:			17. LIMITATION OF ABSTRACT	18. NUMBER OF PAGES	19a. NAME OF RESPONSIBLE PERSON
a. REPORT	b. ABSTRACT	c. THIS PAGE			Traian Dogaru
Unclassified	Unclassified	Unclassified	UU	62	19b. TELEPHONE NUMBER (*Include area code*) (301) 394-1482

Standard Form 298 (Rev. 8/98)
Prescribed by ANSI Std. Z39.18

Contents

List of Figures

List of Tables

Acknowledgments

I would like to acknowledge the contribution of Dr. DaHan Liao from the U.S. Army Research Laboratory (ARL), who performed the FEKO simulations as well as created the synthetic aperture images in this report.

1. Introduction

Over the last decade, the RF Signal Processing and Modeling Branch at the U.S. Army Research Laboratory (ARL) has invested significant resources in developing computational electromagnetic (CEM) modeling tools based on the finite difference time domain (FDTD) method. The AFDTD software for radar signature calculations is the main result of these efforts. A thorough description of the AFDTD software along with an introduction to the FDTD algorithm was presented in reference 1.

A major limitation of the original AFDTD code is that it only considers scenarios where targets are placed in the far-field zone of the radar transmitter and receiver. While this configuration is appropriate for many radar applications, there are other situations (described later in this report) where the far-field assumption may not be valid. In such cases, a near-field FDTD code, which includes the radar transmitter and receiver inside the computational domain, must be used to model the radar scattering process. Recent efforts in this direction led to the development of a near-field, FDTD-based software, called NAFDTD.

NAFDTD is built upon the AFDTD software framework, with which it shares many common features. Both programs are three-dimensional (3-D) electromagnetic (EM) solvers specifically designed for radar scattering problems in a half-space environment. They allow one to calculate a target's time- or frequency-domain signature in response to a short pulse excitation, which is ideal for modeling ultra-wideband (UWB) radar systems. The codes can handle almost arbitrary media electric properties and geometries. Note that the computational grid structure specific to the AFDTD code is entirely preserved for the NAFDTD code. Additionally, both programs are fully parallelized using the message passage interface (MPI) framework. This allows the user to take advantage of the huge computing power available at the High-Performance Computing (HPC) Centers. At the same time, NAFDTD inherits the disadvantages associated with the FDTD method, especially the large requirements in terms of computational resources, as well as problems related to the staircase approximation of curved boundaries between different materials. Moreover, the near-field configuration introduces some new, challenging numerical issues (particularly for radar scattering problems) that are not present in the far-field case.

This report is organized as following: section 2 emphasizes the differences between the near- and far-field EM modeling scenarios and presents typical applications of the former; section 3 discusses the specific numerical issues related to the near-field FDTD code; section 4 represents a user's guide to running the NAFDTD software; section 5 describes a utility program that helps generating the sources and receivers for the NAFDTD software; in section 6, we perform a code validation and show several examples of using NAFDTD; and we finish with conclusions and plans for future work in section 7.

2. Near-Field Versus Far-Field in FDTD Modeling

2.1 The Equivalence Principle in EM

Since the implementation of the EM radiation sources and receivers in the FDTD codes relies heavily on the equivalence principle (*2*), we start by describing it briefly. Although there are many ways of formulating the equivalence principle in EM, we are mainly interested in Love's formulation, illustrated in figure 1. This theorem states that we can replace all the sources (primary and secondary) located inside or outside a closed surface by the tangential field components on that surface, without changing the resulting fields in the complementary region of space.

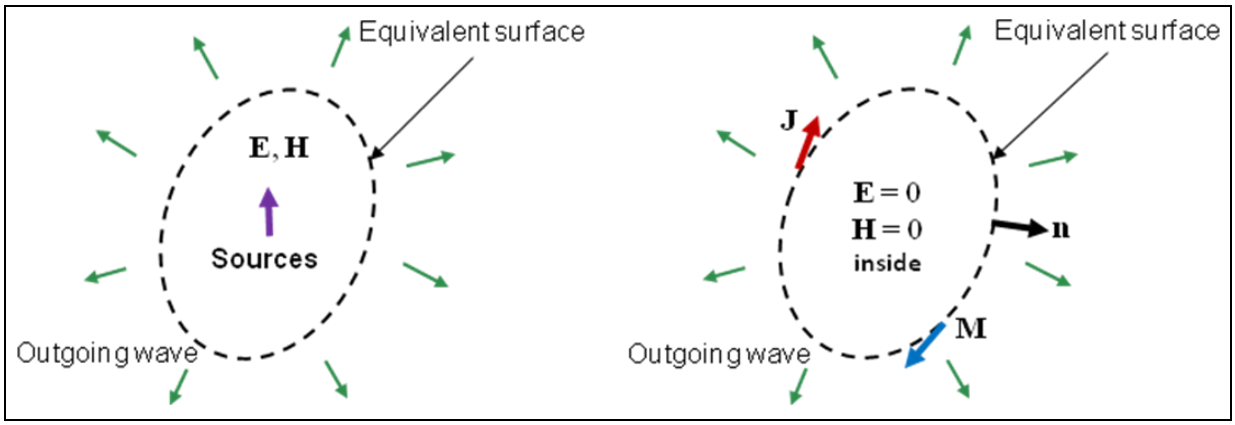

Figure 1. Illustration of the equivalence principle in EM. The fields outside the equivalent surface are identical when the currents **J** and **M** satisfy equations 1 and 2.

The tangential field components are typically associated with surface current densities **J** (electric) and **M** (magnetic) according to

$$\mathbf{J} = \mathbf{n} \times \mathbf{H} \tag{1}$$

$$\mathbf{M} = -\mathbf{n} \times \mathbf{E} \tag{2}$$

where **n** is the normal to the equivalent surface (in figure 1 this is pointed in outward direction). Notice that **J** and **M** are mathematical objects and do not have to correspond to physical currents. At the same time, the equivalent surface does not have to coincide with any specific physical boundary.

Throughout this report, we call the surfaces associated with the equivalence principle—Huygens boxes (reminiscent of the Huygens principle (*2*), which is a simplified version of the equivalence principle).

2.2 Near-Field Versus Far-Field in EM Modeling

In EM theory, one can distinguish between near- and far-field wave propagation. In general, given a source of EM radiation (such as an antenna or a scatterer), the approximate boundary between the two regions depends on the source physical size D and the wavelength λ according to (*2*)

$$r = \frac{2D^2}{\lambda} \tag{3}$$

where r is the distance from the source. In the far-field region, the wave propagation can be locally approximated by a plane wave, which significantly simplifies the analysis. Thus, a plane wave propagates in a ray-like manner and supports a transversal electromagnetic (TEM) mode, where the electric and magnetic vector fields are perpendicular to each other and also perpendicular to the direction of propagation. These assumptions are generally not valid for near-field propagation, where the exact solution of Maxwell's equation is required in order to obtain all six components of the field.

Since the FDTD algorithm provides the exact (or full-wave) solution of the EM field in a given region of space, it can always be applied to the near-field analysis of that region. In the case of a radar scattering scenario, the computational domain would include the transmitter (or radiating source), the receiver and the target (see figure 2a). However, if the radar transmitter is placed far away from the target (according to reference 3) the incident fields that reach the vicinity of the target can be approximated with a plane wave (figure 2b). When the background media configuration is relatively simple (such as the air-ground half-space shown in figure 2b), the incident fields in the target vicinity can be computed analytically, while the source is removed outside the computational domain. This avoids the costly numerical computation of the wave propagation from source to target and allows the computational domain to be truncated to a small region around the target. The full implementation of this procedure involves the analytic computation of the incident fields on a Huygens box around the target and the propagation of those fields inside the box and is known as the split field approach for creating the excitation (*3*).

A similar (though reversed) procedure can be applied to account for the scattered wave propagation from the target back to the radar receiver, in the assumption that these are spaced out at a large distance. This time, the scattered fields radiated by the target in its vicinity are collected on a Huygens box and propagated analytically to the far-zone receiver placed outside the computational domain. This is known as the near-to-far zone transformation (*3*). Both the split field implementation and near-to-far zone transformation are part of the AFDTD (far-field) code (figure 3). Notice that the FDTD numerical computations still occur in the near-field area around the target. However, characteristic to the far-field implementation is the fact that the sources and receivers are removed outside the computational domain, with analytic calculations accounting for the propagation of the incident fields from source to target and the scattered fields from target to receiver.

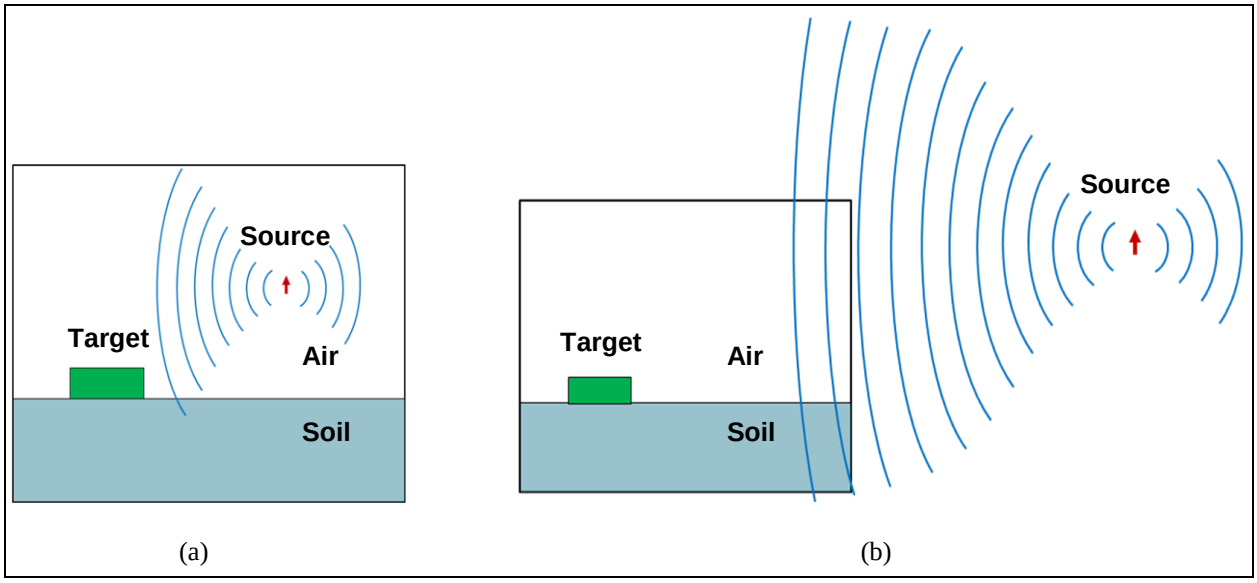

Figure 2. FDTD computational domain showing a target in an air-soil environment, for the (a) near-field case (source inside the computational domain) and (b) far-field case (source outside the computational domain)

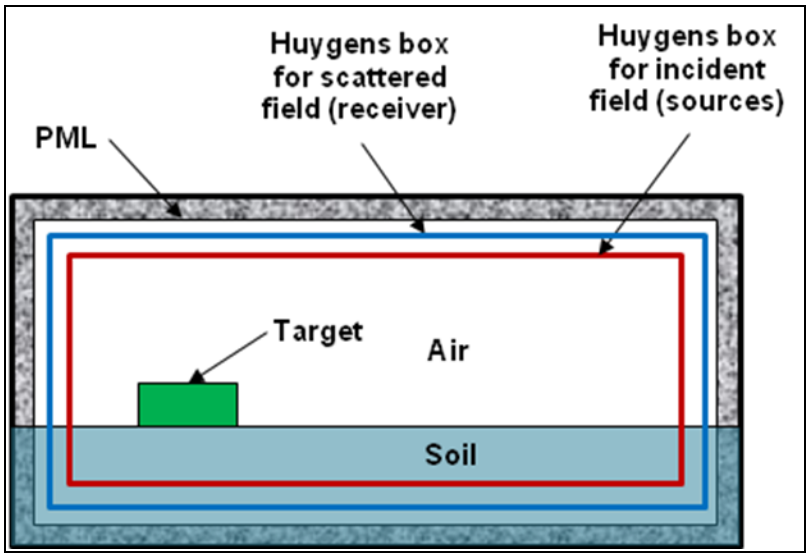

Figure 3. FDTD implementation of the plane wave excitation and the near-to-far zone transformation for the far-field version of the code.

In the case of the NAFDTD code, the source(s), receiver(s), and target(s) are all included inside the computational domain, and therefore, all the propagation and scattering phenomena are accounted for numerically. This type of "brute force" approach to EM modeling of a radar scenario usually requires larger computational resources and should only be used when the far-field assumptions are not valid.

2.3 Source and Receiver Implementation in the Near-field FDTD Code

As described in reference 1, the FDTD equations represent discrete versions of Maxwell's curl equations in the time domain. If one includes the EM radiation sources, the equations updating the E_z and H_z field components can be written as

$$E_z^{n+1}(i,j,k) = E_z^n(i,j,k) + \frac{\Delta t}{\varepsilon \Delta x}\left[\begin{array}{l} H_y^{n+1/2}(i,j,k) - H_y^{n+1/2}(i-1,j,k) - \\ -H_x^{n+1/2}(i,j,k) + H_x^{n+1/2}(i,j-1,k) \end{array}\right] - \frac{\Delta t}{\varepsilon} J_z^{n+1}(i,j,k) \qquad (4)$$

$$H_z^{n+1/2}(i,j,k) = H_z^{n-1/2}(i,j,k) + \frac{\Delta t}{\mu \Delta x}\left[\begin{array}{l} E_x^n(i,j+1,k) - E_x^n(i,j,k) - \\ -E_y^n(i+1,j,k) + E_y^n(i,j,k) \end{array}\right] - \frac{\Delta t}{\mu} M_z^{n+1/2}(i,j,k) \qquad (5)$$

where Δx is the cell size (assumed the same in all directions), whereas Δt is the time step. The quantities J_z and M_z represent the z components of the impressed electric current density (measured in A/m^2) and magnetic current density (measured in V/m^2). They may represent real physical quantities (e.g., the electric current along a wire antenna) or mathematical objects that result from the application of the equivalence principle. Notice that, for grid cells that do not include sources, the last term in equations 4 and 5 is set to zero.

Equations 4 and 5 describe the implementation of so-called *soft* sources in the FDTD algorithms (*3*). The less accurate alternative is to implement *hard* sources, where certain field components are forced to specific values during the FDTD time-marching procedure.

Although the EM radiation source in the radar model is represented by an antenna, the NAFDTD software avoids the inclusion of a direct physical antenna model. Instead, the antenna is replaced by current densities (physical or equivalent) that create the same field distribution throughout the computational domain. The current density spatial distribution representing the radiation source is discretized consistently with the FDTD rectangular grid, in effect creating a collection of small dipoles of length Δx. The advantages of this procedure are: a simple and uniform way of specifying the sources as an input to the code; and the fact that these *soft* sources do not interfere with the propagation of the scattered field. The disadvantage consists of having to perform the extra step of determining the current densities that replace the antenna (either by analytic or numeric methods).

In some cases (particularly wire and patch antennas), the radiating elements can be replaced by the physical electric current densities induced along their conducting surfaces. For example, wire antennas can be replaced by the electric current intensity (in A) distribution along the one-dimensional wire geometry, while patch antennas can be replaced by the electric surface current density (in A/m) induced along the two-dimensional conducting surface. In other cases (such as aperture, slot, or notch antennas), the EM radiation can be described by applying the equivalence principle and replacing the antenna physical structure by equivalent current densities along appropriate surfaces (e.g., the open-end surface of a waveguide or horn antenna [*2*]). The main issue with the approaches described in this paragraph is that, when the antenna geometry does

not conform to the Cartesian axes or planes, the current density spatial distributions are difficult to describe and are subject to possible staircase approximation errors.

A more general approach to implementing the radiation sources placed within the computational domain is based on introducing Huygens boxes around the radiating elements and applying the equivalence principle (figure 4). The radiating elements (transmitting antennas) are completely enclosed by the Huygens box and replaced by the equivalent currents along the surfaces of the box. Note that the Huygens box always has rectangular shape and conforms to the Cartesian geometry of the FDTD grid; therefore, non-conformal antenna geometries can be handled by this approach without worrying about staircase approximation errors. As compared to the Huygens box that implements the excitation in the far-field code (figure 3), where the fields are propagated inwardly, the near-field code requires an excitation Huygens box that propagates the fields outwardly.

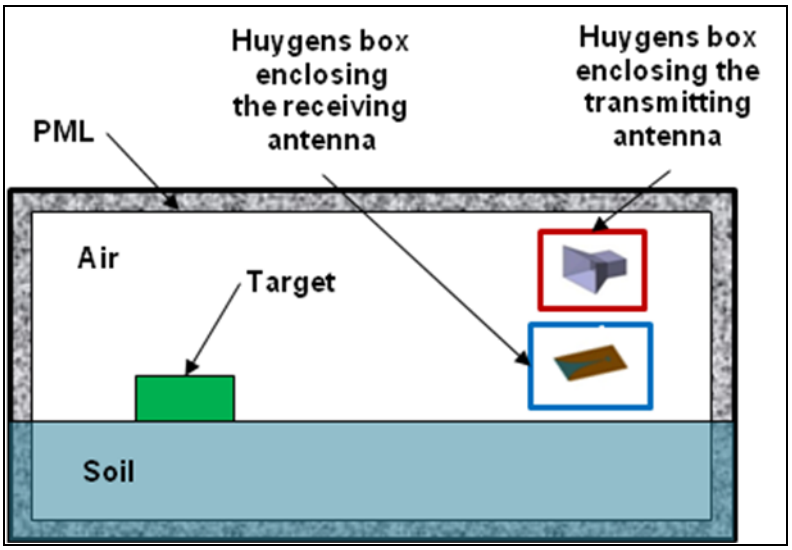

Figure 4. FDTD implementation of the transmitting and receiving antennas via Huygens boxes and the equivalence principle for the near-field version of the code.

As previously mentioned, a major problem with implementing this approach is the calculation of the equivalent current densities (or tangential field components) along the Huygens box. Except for very simple cases, the fields in the neighborhood of an antenna cannot be computed exactly via analytical methods (note that this is a near-field calculation, so asymptotic far-field approximations for calculating antenna patterns do not apply). The only reasonable general solution to this problem is performing a separate numerical simulation of the transmitting antenna by means of a specialized antenna modeling software. Accurate results on antennas with complicated geometries can be obtained by integral equation (also known as method-of-moments [*2*]) techniques, such as those implemented by the FEKO software package (*4*).

An analogous procedure can be applied to compute the output of a receiving antenna. In general, the FDTD algorithm produces the time samples of the electric and magnetic field components at the grid nodes. However, in a radar system model, we are mainly interested in the voltage at the receiving antenna terminals. As with the radiating antenna, the transformation from the field components in the receiving antenna neighborhood to the voltage at its terminal is a non-trivial task that must be handled by a specialized numerical code outside the FDTD program. The receiving antenna is completely enclosed by a Huygens box (figure 4) where the equivalent currents (or tangential fields) are calculated at each time step by the FDTD algorithm. These tangential field components are used as an input to a receiving antenna simulator (e.g., FEKO) to compute the voltage at the terminal. Notice that the fields inside the receiving Huygens box propagate inwardly.

Regardless of the method for describing the radiating elements in the radar model, the excitation sources for the NAFDTD code are always organized as a collection of small electric and magnetic dipoles of length Δx as excitation sources. If the magnitude of one dipole's electric current or magnetic moment (*2*) is *A*, then the corresponding electric or magnetic current density at that grid point (*J* or *M* in equations 4 and 5) is $\frac{A}{\Delta x^3}$.

Similarly, the receivers are described as a collection of grid points where all the field components are probed during the time-marching process. The structure of the input and output files associated with the sources and receivers is detailed in section 4. A utility program called SOURCERECEIVER that helps generate the input files associated with the sources and receivers is described in section 5.

2.4 Near-field Versus Far-field in Radar Imaging

Synthetic aperture radar (SAR) imaging represents a major application for our research group at ARL. Many of our numeric radar scattering modeling results have been used as input data in SAR imaging studies (*5*–*7*). In this section, we emphasize the differences between near- and far-field SAR image formation algorithms and the requirement to produce radar modeling data consistent with the geometry of the imaging system.

Regardless of the SAR system configuration (spotlight or strip-map [*8*]), the image can be created by applying the backprojection algorithm (BPA) (*8*). In its most basic form (also known as "delay-and-sum"), the image pixel intensity at coordinates (*x*, *y*) can be calculated as

$$I(x,y) = \sum_{n=1}^{N} s_n\left(\tau_n(x,y)\right) \tag{4}$$

where s_n is the time-domain signals at the n^{th} receiver position along the synthetic aperture and τ_n is the time delay characterizing the propagation from transmitter to image pixel and back to the receiver (for simplicity, we assume monostatic radar configuration).

The difference between the far- and near-field geometry is illustrated in figure 5. In figure 5a (far-field), we notice the planar wavefront coming from and going to the radar antenna, with parallel rays connecting the radar position to any pixel in the image. In figure 5b (near-field), the wavefronts are spherical, with divergent rays connecting the radar position to the image pixels. The delay τ_n is given by the general expression

$$\tau_n(x,y) = \frac{2R_{Pn}}{c} = \frac{2\sqrt{(x-x_n)^2 + (y-y_n)^2}}{c} \tag{6}$$

where c is the speed of light, and x_n and y_n are the Cartesian coordinates of the n^{th} radar position on the aperture. This equation is valid for any type of radar geometry. However, for the far-field case, the delay can be expressed as a function of the polar coordinates of the radar position, R_{0n} and ϕ_n, as

$$\tau_n(x,y) = \frac{2R_{Pn}}{c} = \frac{2R_{0n}}{c} - \frac{2(R_{0n} - R_{Pn})}{c} = \frac{2R_{0n}}{c} - \frac{2(x\cos\phi_n + y\sin\phi_n)}{c} \tag{7}$$

A common far-field assumption is that R_{0n} is constant with n (the aperture is circular), such that the $\frac{2R_{0n}}{c}$ term does not have any effect on the image pixel magnitude. In this case, the only relevant geometrical parameter in equation 7 is the angular position of the radar on the aperture. Most far-field algorithms for SAR image formation, including BPA and the polar format algorithm (*8*), are range independent and base their delay calculation directly on equation 7.

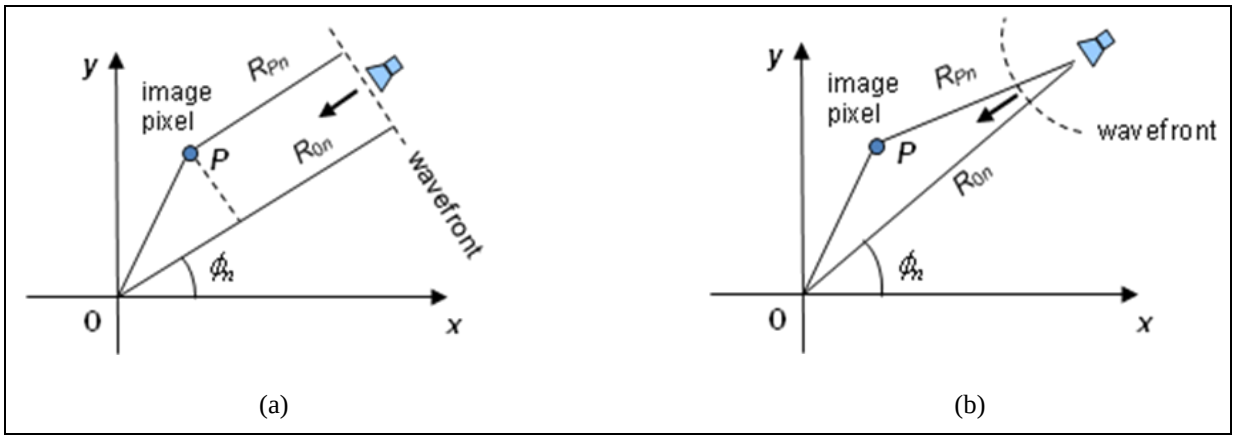

Figure 5. Geometry of the calculation of the delay τ_n in the SAR image formation algorithm for the (a) far-field case and (b) near-field case.

Notice that, in general, it is not possible to reduce the expression in equations 6 to 7, except for the case when x_n and y_n are much larger than x and y. It is apparent from the diagrams in figure 5, as well as the equations 6 and 7, that the EM modeling data must be consistent with the imaging algorithm in order to avoid significant distortions in the SAR image (meaning that far-field model data must be associated with the far-field imaging algorithm, whereas the near-field model data must be associated with the near-field imaging algorithm).

A radar imaging application that has received a great deal of attention at ARL is that of terrain-mapping by forward-looking radar (*9*). In this application, a physical antenna array placed on a vehicle and elevated from the ground scans the terrain for obstacles near the ground surface, while the vehicle moves forward (figure 6).

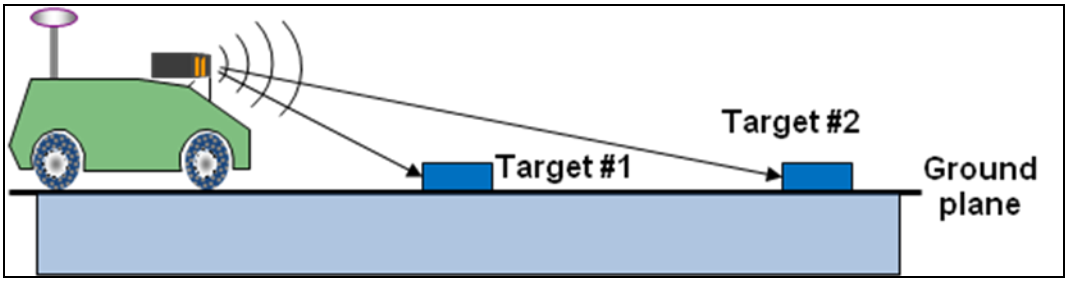

Figure 6. Schematic representation of the forward-looking radar configuration for imaging two identical targets placed at different ranges.

Let us assume that the vehicle is stationary and the image of the two identical targets in figure 6 is created via a time-reversal algorithm (*10*) based on the data collected by the physical aperture consisting of 2 transmitting antennas and 16 receiving antennas (such as the configuration described in reference 9). Without getting into the details of this simulation, the images obtained for the far-field (figure 7a) and near-field (figure 7b) configurations display significant differences. Thus, the images of the two targets look identical in figure 7a (independent of range), while showing differences in intensity, cross-range resolution, and sidelobe curvature in figure 7b. (For the record, the imaging algorithm for the near-field case compensates for the range path loss; the intensity difference between the two targets is produced by different elevation look angles by the radar; at the same time, the targets are seen at the same elevation angle in the far-field case).

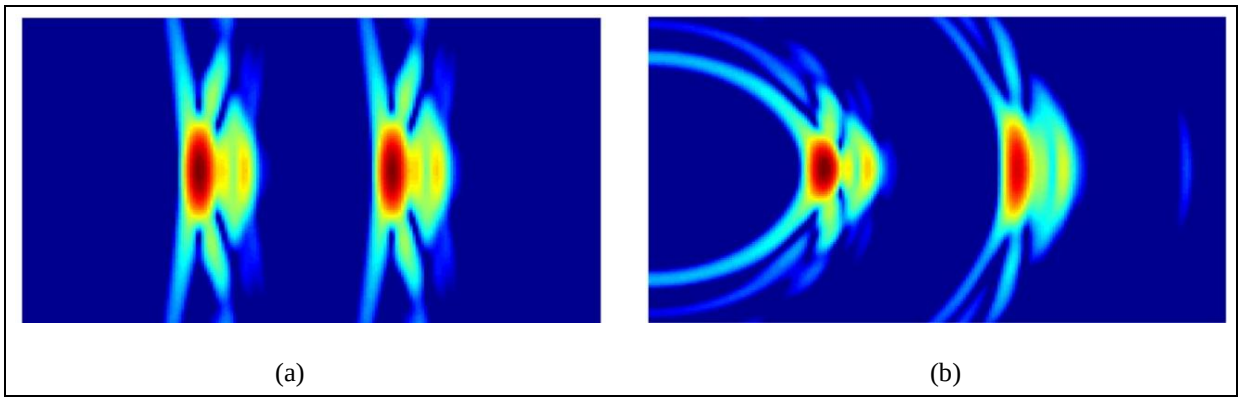

Figure 7. SAR images obtained for the configuration shown in figure 6 for the (a) far-field case and (b) near-field case.

This example demonstrates that the near- and far-field configurations generally create different EM scattering phenomenology and that one configuration cannot be easily reduced to the other. It also provides a rationale for developing two separate FDTD modeling codes, one for far-field

and one for near-field radar simulations. Table 1 summarizes the similarities and especially the differences between the two configurations, as relevant to the FDTD radar scattering models and the SAR imaging algorithms.

Table 1. Comparison between the far-field and near-field FDTD codes.

Far-field FDTD model	Near-field FDTD model
Targets inside the computational domain	Targets inside the computational domain
Sources and receivers outside the computational domain	Sources and receivers inside the computational domain
Plane wave excitation	"Spherical" wave excitation
Propagation geometry defined by angles of incidence and scattering	Propagation geometry defined by 3-D coordinates of transmitters and receivers
The absolute range from radar to target is not included in the solution	The absolute range from radar to target is part of the solution ("range path loss")
The antenna pattern is not part of the model	The antenna pattern is included in the model
Reduced size of the computational domain	More accurate model of the EM problem
Typically associated with circular spotlight SAR	Typically associated with linear strip-map SAR
Imaging algorithm uses only pixel positions and propagation angles	Imaging algorithm uses distances between pixels and radar positions

2.5 Applications of the Near-field FDTD Code

There are numerous radar applications that require a near-field EM scattering analysis (meaning that they cannot be reduced to the far-field case). Many of them are related to radar imaging of targets in the vicinity of an air-ground interface (above or below the ground surface). Researchers at ARL have been investigating the detection of these targets using techniques such as forward-looking, ground penetrating, or borehole radar. This section briefly describes several applications where the NAFDTD software can be used in EM field modeling, including radar system analysis.

One problem of interest is terrain-mapping using forward-looking radar (figure 8). The antenna assembly in mounted on a vehicle that drives forward, while a radar image of the terrain in front of the vehicle is created. The purpose is the standoff detection of obstacles and possible explosives (landmines, improvised explosive devices, unexploded ordnance) along the driving path. This configuration is characteristic to the Synchronous Impulse Reconstruction (SIRE) radar, described in reference 9.

The configuration described in figure 8 has been modeled using the AFDTD far-field code, with results reported in reference 7. The study was centered around modeling the surface clutter created by the rough terrain and quantifying its impact on target detectability. However, given the relatively short operational range of the SIRE radar (from 8 to 33 m) and the large size of the image area, this problem can be more accurately described by a near-field configuration. Additionally, the near-field FDTD code would allow taking into account the antenna patterns in the EM scattering model. A preliminary study of the forward-looking radar using the NAFDTD code was performed in reference 10. Figure 9 displays the terrain images obtained with the stationary radar for the cases when the ground surface is flat (figure 9a) and rough (figure 9b).

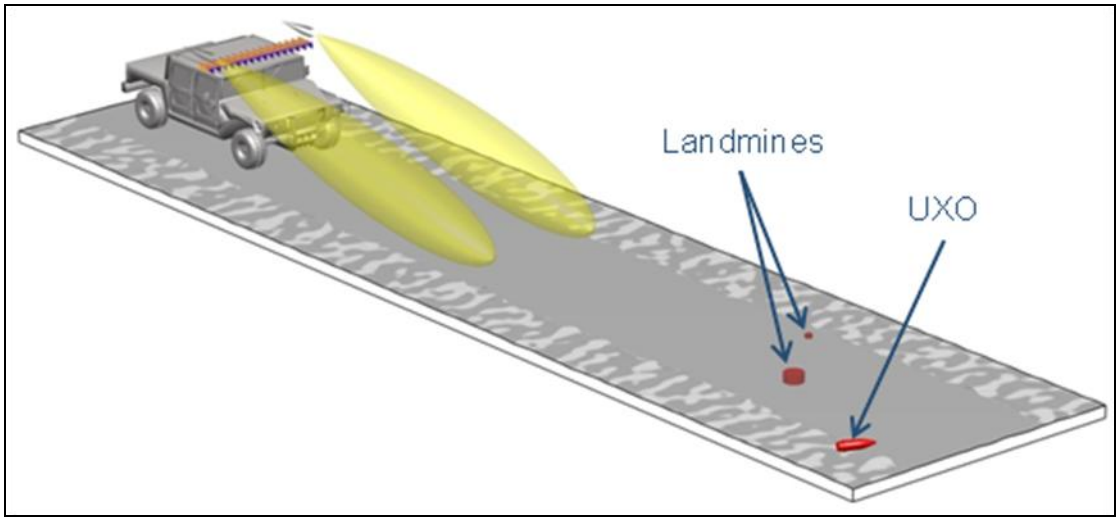

Figure 8. The forward-looking SIRE radar in terrain-mapping configuration.

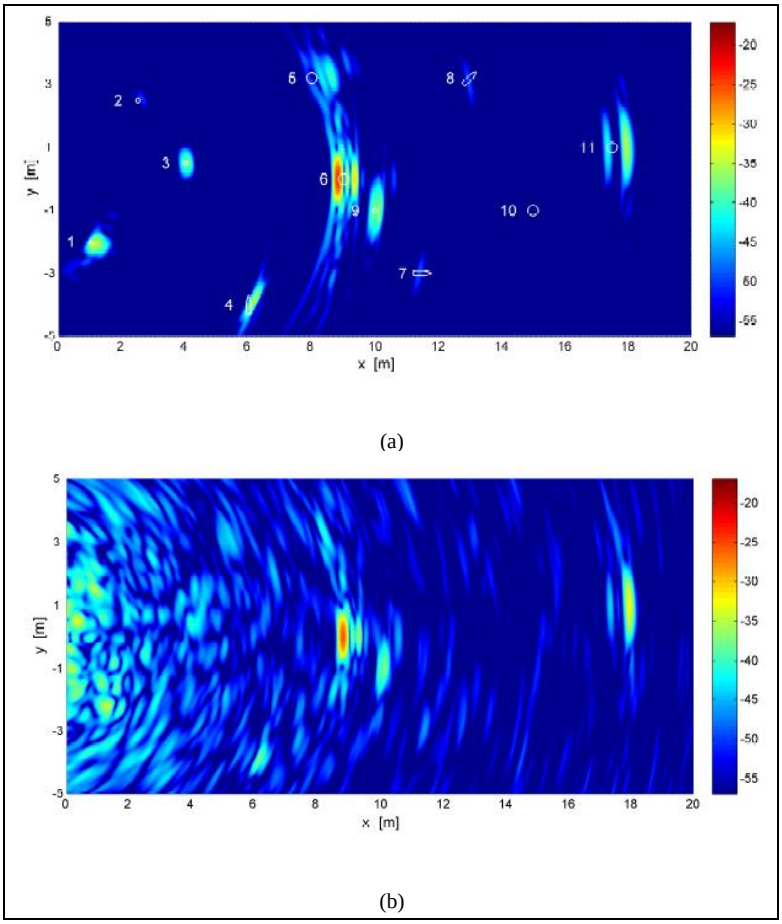

Figure 9. SAR images based on the near field NAFDTD code simulating the SIRE radar operation for (a) flat air-ground interface and (b) rough air-ground interface.

Ground-penetrating radar (GPR) represents another important application where the proximity between radar antennas, ground interface, and target requires a near-field EM analysis. An example of down-looking GPR mounted on a vehicle for road-clearing operations is the Non-Intrusive Inspection Technology (NIITEK) radar (*11*). A near-field FDTD model of this configuration was reported in reference 12, along with 3-D images of buried targets created from modeling data (figure 10).

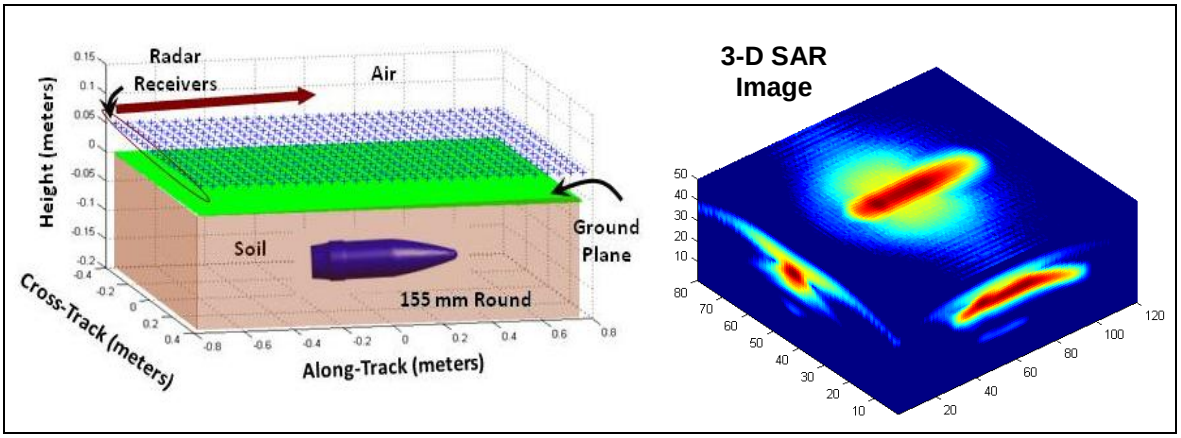

Figure 10. A 3-D image of a buried 155-mm round based on the near-field FDTD model of a down-looking GPR system.

Another possible near-field-type radar application is detection of deep underground objects (such as a metal pipe) using borehole radar (figure 11). A SAR imaging study based on data collected by borehole radar at ARL was reported in reference 13. Part of that study consisted of models performed by the near-field FDTD code. Imaging results showing the unfocused and focused radar images of a steel pipe are displayed in figure 12.

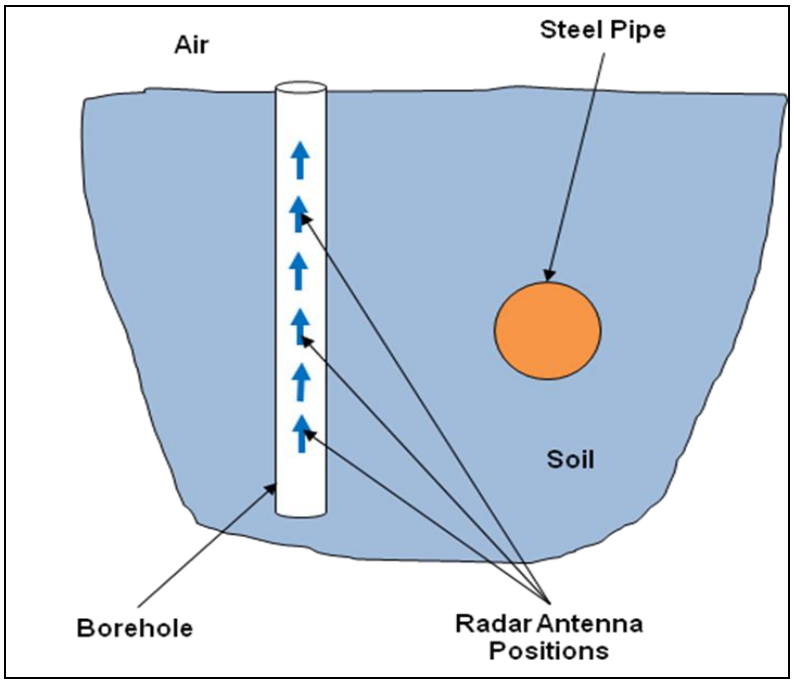

Figure 11. Schematic representation of a borehole radar system for deep buried object detection.

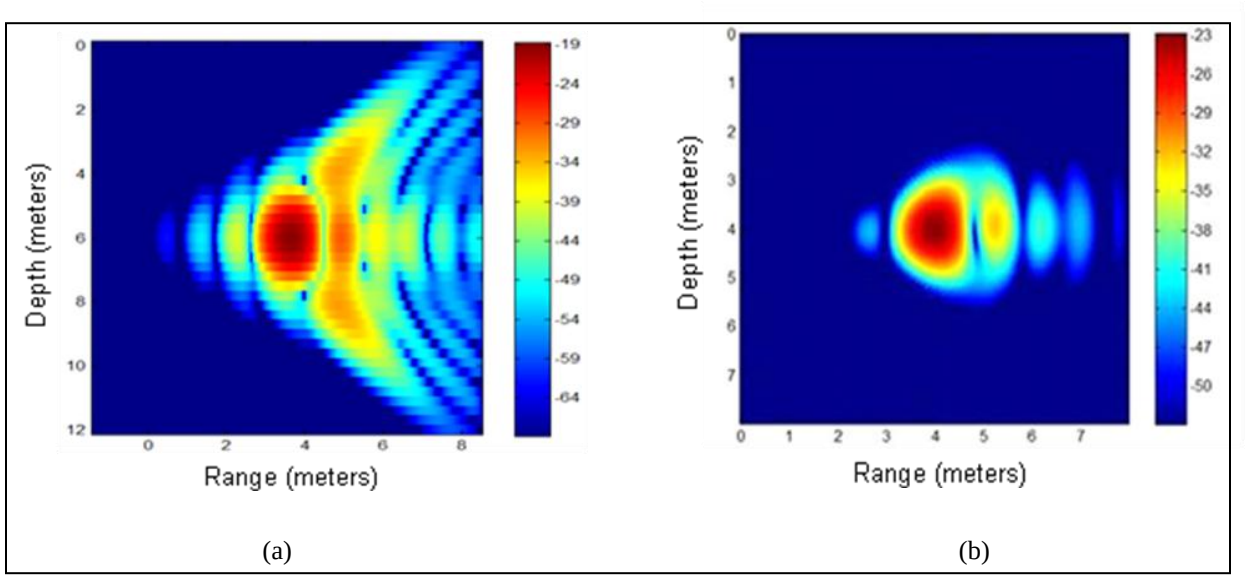

Figure 12. Examples of target scattering data based on a borehole radar FDTD model showing (a) unfocused (raw) radar data and (b) focused SAR image.

Sensing through the wall (STTW) radar has received considerable interest from Defense agencies over the last few years. ARL has performed several modeling studies to predict imaging radar performance in an urban environment (*5*, *6*). Most of these studies employed the AFDTD far-field modeling code to the EM scattering problem analysis. Although these simulations have led to some important phenomenological insight, not every STTW radar imaging scenario can be correctly characterized as far-field geometry. As shown in reference 5, the near-field zone of a large building may extend up to 400 m away at frequencies typical to this application. Therefore, a strip-map SAR imaging system mounted on a vehicle driving on a road nearby a building (figure 13), is more accurately modeled by a near-field EM solver such as NAFDTD.

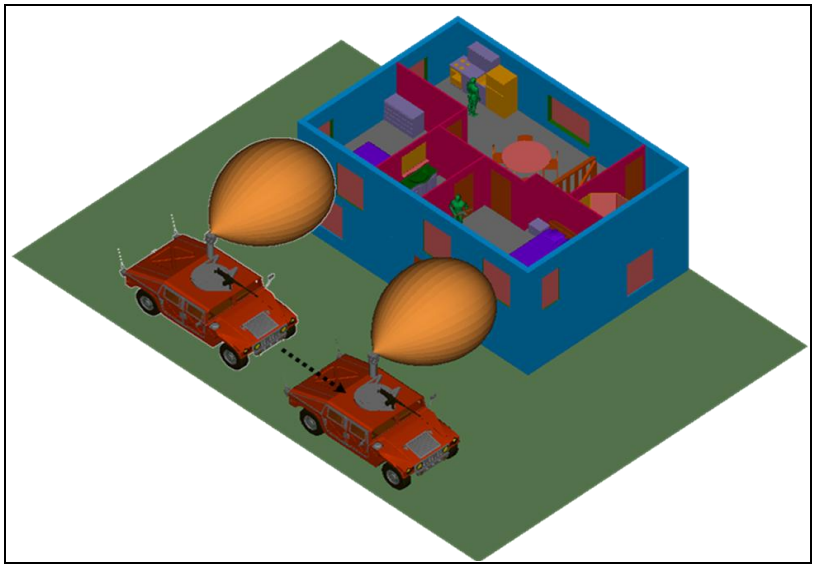

Figure 13. Strip-map SAR imaging of a building using a side-looking radar mounted on a vehicle.

While all the modeling applications mentioned so far are related to radar systems, near-field FDTD analysis can be extended to many other EM problems (a comprehensive list is presented in reference 3). Two possible applications of interest to our research group are antenna analysis (figure 14) and microwave RF circuit analysis (figure 15). Given the limitations of the AFDTD/NAFDTD framework (particularly the staircase approximation of the boundary), accurate analysis of these type of structures would most likely be restricted to planar (strip or microstrip) geometries. One example of planar antenna geometry that is a good candidate for NAFDTD modeling is the Vivaldi antenna, which has important applications in UWB radar.

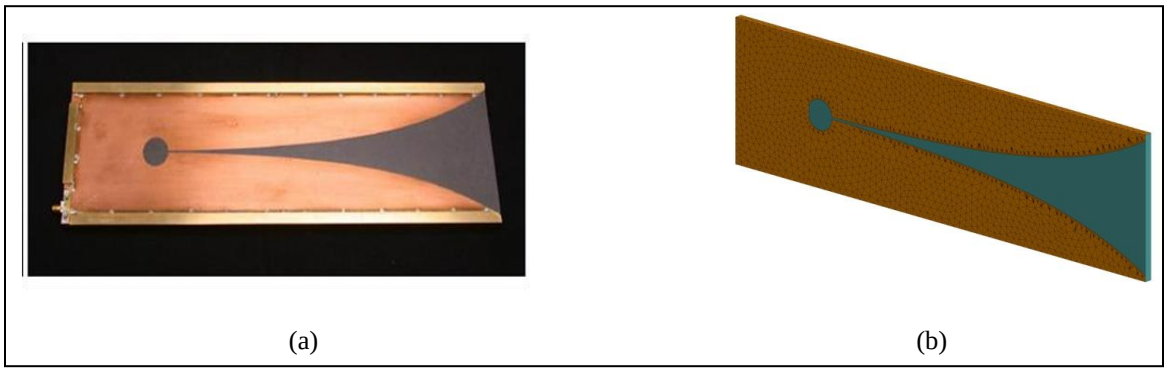

(a) (b)

Figure 14. UWB Vivaldi notch antenna showing (a) physical structure and (b) mesh for computer modeling.

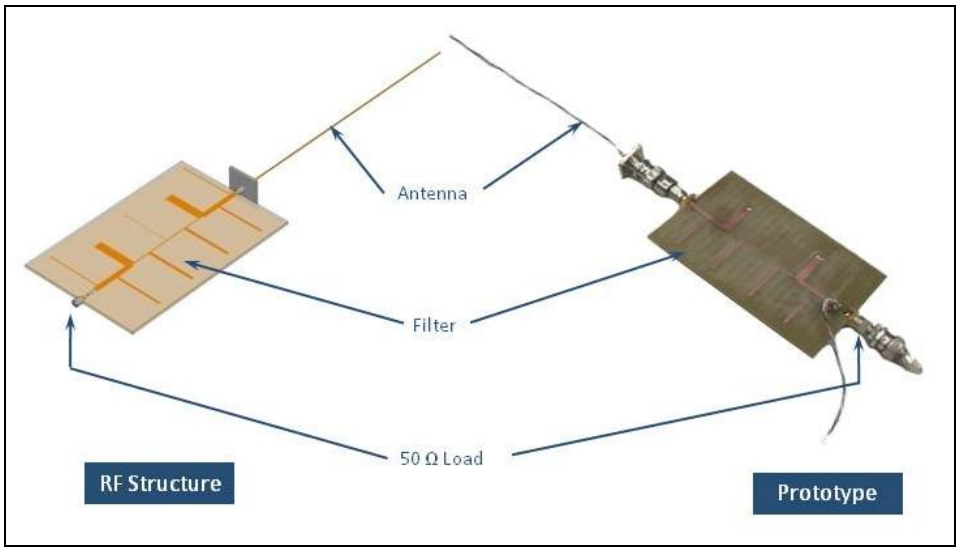

Figure 15. Passive RF circuit that could be modeled by the NAFDTD code.

3. Numerical Issues Related to the Near-field FDTD Code

As already mentioned, the general FDTD algorithm is affected by certain numerical issues—primarily, the numerical dispersion and the staircase approximation of material boundaries—that

limit its accuracy. Additionally, the near-field FDTD code presents several new challenges that are not relevant to the far-field version. The differences arise from the ways the radiation sources and receivers are implemented in the two configurations. In this section, we discuss these challenges and point to possible mitigation techniques.

3.1 Modeling Radar Scattering with NAFDTD

As well known in EM wave theory (*2*), the field intensity away from a localized radiation source varies approximately as $1/R$ in free-space (where R is the distance from the source). Therefore, the EM signal scattered by a radar target placed at a large distance from the radar antennas could be many orders of magnitude weaker than the direct fields radiated in the vicinity of the transmitter. Since the radar receiving antenna is typically placed in this vicinity, a good isolation between the direct transmitter-receiver signal and the target-scattered signal is a critical feature of any radar system (*14*). One way to achieve this is by transmitting short pulses and separating the aforementioned signals in the time domain. Another mitigation solution is choosing a physical and geometrical configuration that minimizes the direct EM leakage between the transmitting and receiving antennas.

This issue is relevant to a computer program that simulates radar scattering as well. Since NAFDTD uses soft sources and does not include the physical antenna models (as explained in section 2), the direct radiation between the transmitter and receiver cannot be blocked away. Moreover, the time-domain separation between the direct and scattered signal may not always be possible, because small residual errors in the direct signal may completely swamp the scattered signal. To illustrate this point, consider the following example.

We simulated the scenario described in figure 16, where the radar antennas are represented by small vertical dipoles (in this case, 8 mm long), placed at 2 m above a dielectric ground plane ($\varepsilon_r = 6$, $\sigma = 0.01$ S/m) and 2-cm spacing between the transmitter and receiver. The target is a perfect electric conductor (PEC) cylinder of 30 cm diameter and 16 cm height, whose center is at a range of 18.24 m from the radar transmitting antenna. The transmitter is excited with a current density described by a short-pulse 4^{th} order Rayleigh pulse (*15*) with a center frequency of 500 MHz. Figure 17a displays the total vertical electric field intensity (E_z component) at the receiver, in the time domain. The only feature noticeable in this graph is the direct pulse propagating from the transmitter to receiver, around $t = 0$. The return from the target is shown in figure 17b (around $t = 120$ ns). Notice that, although the two signals are well separated in the time domain, the scattered signal is about 150 dB weaker than the direct signal. As such, any minute error in the total fields propagating throughout the computational domain can have a large impact on the accuracy of the scattered signal. A typical error encountered in FDTD simulations is the residual bias produced by the imperfect zero-field initial condition at the time step when the transmitter is turned on.

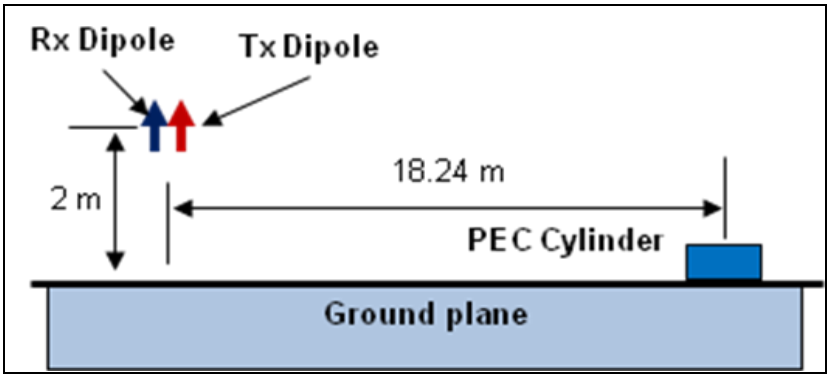

Figure 16. Schematic representation of the geometry for the example illustrating the direct versus scattered field order of magnitude difference.

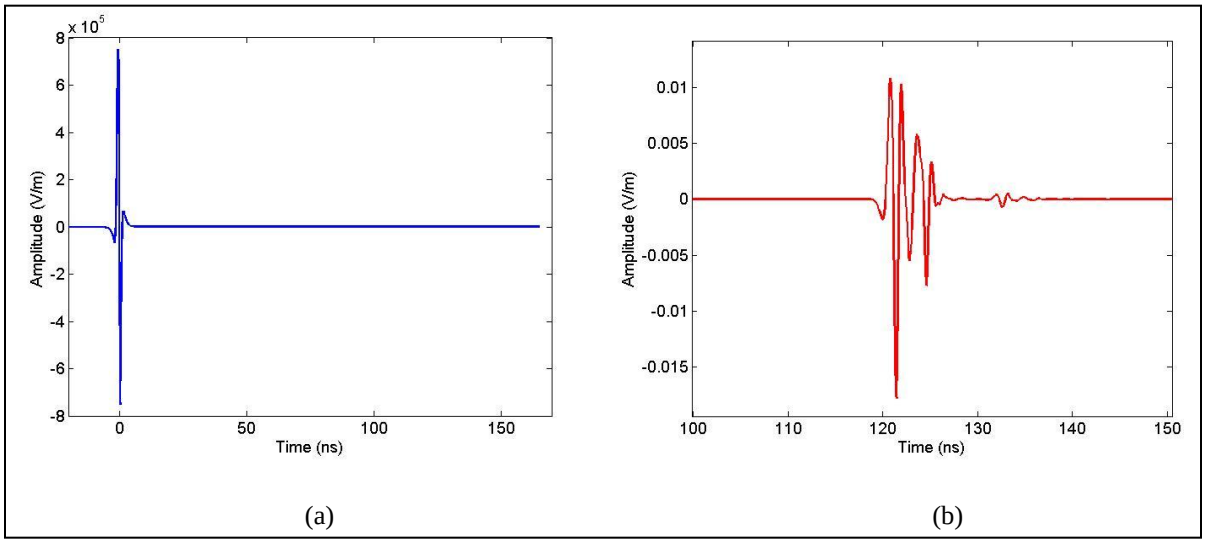

Figure 17. E_z component at the receiver in the time domain for the example in figure 16, showing (a) the overall total field signal and (b) the scattered field only signal.

In order to reliably obtain the target response for any kind of radar scenario, we need to run the simulation twice: the first time including the target and the second time with the background media only (excluding the target). The scattered field is computed as the difference between the field received in the first case ("total field") and the field received in the second case ("incident field"). This way, the direct signal between the transmitter and receiver is exactly cancelled, including any residual artifact caused by it.

This procedure is only required when modeling a radar scattering problem by the near-field FDTD code. If we are simply interested in the radiation problem, where we want to compute the total field that propagates between the transmitter and receiver, we only need to run the simulation once, with the full media configuration. Notice also that this procedure, where the code is run twice, is not required by the far-field FDTD code, where the subtraction of the incident field outside the incident field Huygens box (scattered-fields-only region) is implicit in the algorithm (see figure 3).

An interesting aspect of calculating the fields scattered by a weak target with the near-field FDTD code is that, in some cases, the amplitude of the scattered signal may become comparable to the computer's machine precision. As a reminder, in the standard single precision representation, 24 bits are used to represent a real number's mantissa, meaning that the single precision representation has a dynamic range of 144 dB. If we consider a target placed at 100 wavelengths from the radar, the path loss in free space is about –80 dB. Assuming a weakly scattering target with a radar cross section of –40 dBsm, the scattered-to-direct-field ratio would be –120 dB, which starts to approach the numerical dynamic range of the single precision representation (in reality, the calculation of the scattered-to-direct-field ratio is more complicated; this example just illustrates the point). In simulations where the single precision representation does not offer sufficient dynamic range, double precision may be required.

In figure 18, we further magnify the scattered field waveform obtained for the radar scenario described in figure 16. Notice that the double precision calculation offers the correct answer (and a smooth waveform), whereas, for the single precision calculation, the least significant bit randomly jumps between 0 and 1 creating quantization noise. In most cases, this error will not have a significant impact on the overall target signature; however, for very weak or very distant targets, the effect on the accuracy of the computed scattered fields could be more severe. Also, it is interesting to mention that this "numerical noise" issue present in computer simulations has a correspondent in the real world, namely, the quantization noise produced by the limited dynamic range of the analog-to-digital converter in radar systems that use digital signal processing (*14*).

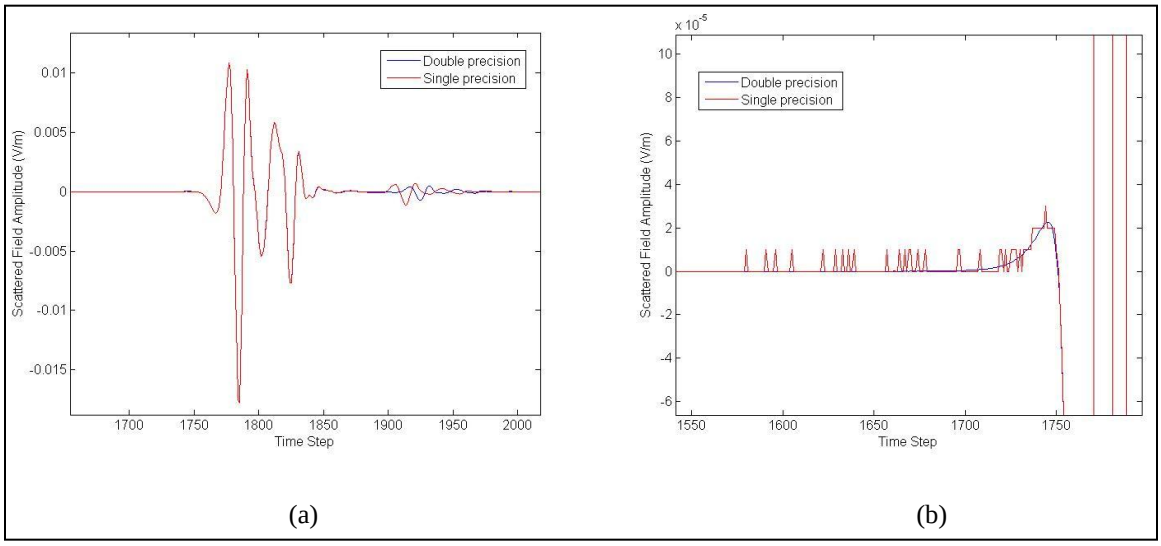

Figure 18. Comparison of the scattered field in the example described in figure 16 computed using single and double precision arithmetic, showing (a) the entire scattered field signal and (b) magnified detail displaying the quantization error for the single precision case.

3.2 Numerical Dispersion in Near-field FDTD Modeling

Numerical dispersion is a computer modeling artifact present in wave propagation simulations, caused by differences between the theoretical and numerical phase velocities of the wave.

Moreover, these differences are frequency-dependent, leading to distortions of wideband pulses propagating over large distances. Although the numerical dispersion is a phenomenon encountered by all explicit FDTD-based algorithms, there are some differences between its effects on the AFDTD (far-field) and NAFDTD (near-field) code.

In the case of the AFDTD code, the excitation ("incident field") is propagated along the incident field Huygens box at the theoretical phase velocity (see figure 3 for reference). However, throughout the rest of the computational domain, the total fields propagate with phase velocities dictated by the numerical FDTD algorithm. The difference between the two phase velocities creates a phase mismatch between the two types of fields. This leads to the incorrect cancellation of the incident field in the scattered-field-only region and, for large computational domains, may show as a late-time extra pulse in the time-domain response of a target (an example of this effect was presented in reference 16). One should be aware that a quantitative spatial analysis of the numerical dispersion error for the far-field FDTD code is very difficult to perform, since the sources are distributed all around the computational domain.

In the case of the NAFDTD code, the radiation sources are typically localized in a small region of the space, so the numerical dispersion analysis is simplified. It has been shown that, for small enough cell sizes, the phase error growth is approximately linear with the distance from the source and the frequency (*3*). In this section, we analyze a large-scale, near-field simulation in order to get a sense of the severity of the numerical dispersion problem.

Consider the configuration in figure 19, where the transmitter is a small vertical dipole of length 8 mm, placed 2 m above a dielectric ground plane ($\varepsilon_r = 6$, $\sigma = 0.01$ S/m). We consider two receiver positions at 18.4 m in horizontal range, one at height $h = 12$ cm and the other at $h = 2$ m above the ground plane, where we probe the vertical electric field (E_z component). We compare the NAFDTD results at different frequencies with those obtained by FEKO (*4*). Note that FEKO uses an integral equation solver, which is not affected by the numerical dispersion issue, so its solution is error-free for this problem. As we can see in the graphs in figure 20, the magnitude of received signals in the NAFDTD simulations matches very well the reference solution (to within fractions of dB) , whereas the phase exhibits errors that increase with frequency. At the maximum frequency considered here (1400 MHz), where the propagation distance is about 85 wavelengths, the phase error is close to 25°. Whether this error level is acceptable depends on the application; however, the error can always be reduced at the expense of a smaller cell size and, consequently, significantly increased computational resources.

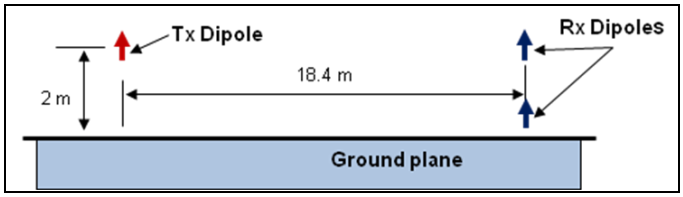

Figure 19. Schematic representation of the geometry for the example used in the quantitative evaluation of the numerical dispersion error.

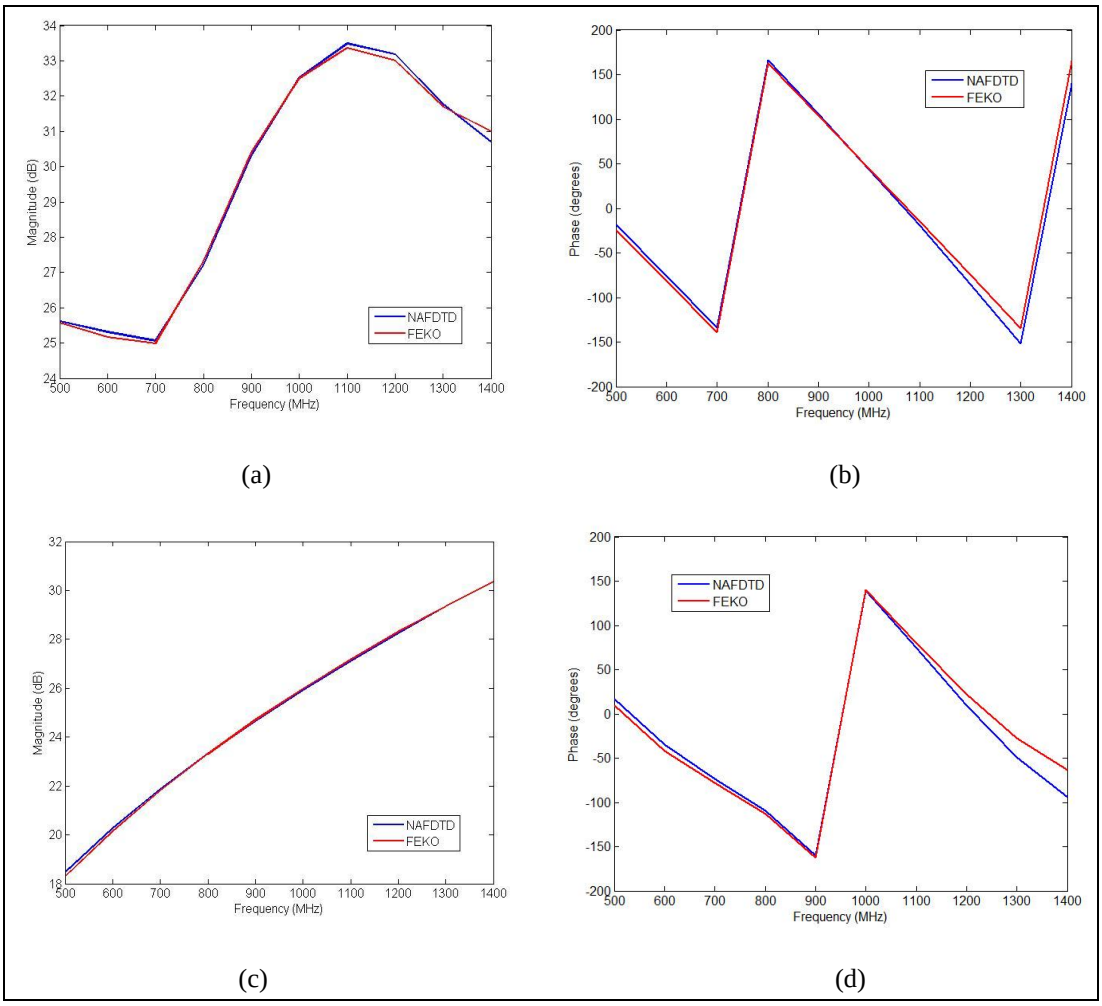

Figure 20. Comparison of the field at the receiver in the example described in figure 19 as calculated by NAFDTD and FEKO showing (a) magnitude at h = 12 cm; (b) phase at h = 12 cm; (c) magnitude at h = 2 m; and (d) phase at h = 2m.

3.3 Perfectly Matched Layer Issues in the NAFDTD Code

The perfectly matched layer (PML) (*17*) is the preferred absorbing boundary implementation in modern FDTD codes. The AFDTD/NAFDTD software uses a version of the split-field PML method adapted to lossy background media, described in reference 18. A typical PML suppresses reflections from the computational domain boundaries by 70–90 dB at normal wave incidence (*3*). As shown in section 3.1, models of scattering from weak targets may require much larger sensitivity—for instance, the fields reflected by a PML located near the source may have much larger magnitude than those scattered by the target and reaching the receiver. However, the subtraction of the "unperturbed" fields by the procedure outlined in section 3.1 effectively cancels such artifacts, so the overall accuracy of the calculation is preserved.

A specific concern related to PML in the context of the near-field FDTD code is the shape factor of the computational domain (by this we mean the ratios of its three dimensions). Since the

attenuation of a plane wave propagating at an angle θ with respect to the normal within a PML varies as $e^{-a\sigma\cos\theta}$, where σ is the PML medium conductivity and a is a constant, it follows that waves propagating close to grazing with respect to a boundary are not well absorbed by the PML (because the factor $\cos\theta$ in the exponent is small). Such a situation can be encountered in the scenario described in figure 21, where the computational domain has a horizontal dimension much larger than the vertical one (by a factor of almost 40). A ray-tracing description of the propagation between the transmitter and receiver for this scenario includes, besides the direct path, the paths reflected by the upper and lower boundaries. Since these reflected waves suffer almost no attenuation through the PML, they have a strong effect on the fields at the receiver location. Figure 22 plots the direct-path-only analytic solution versus the numerical solution obtained for the configuration in figure 21, showing the severe error in the simulated results.

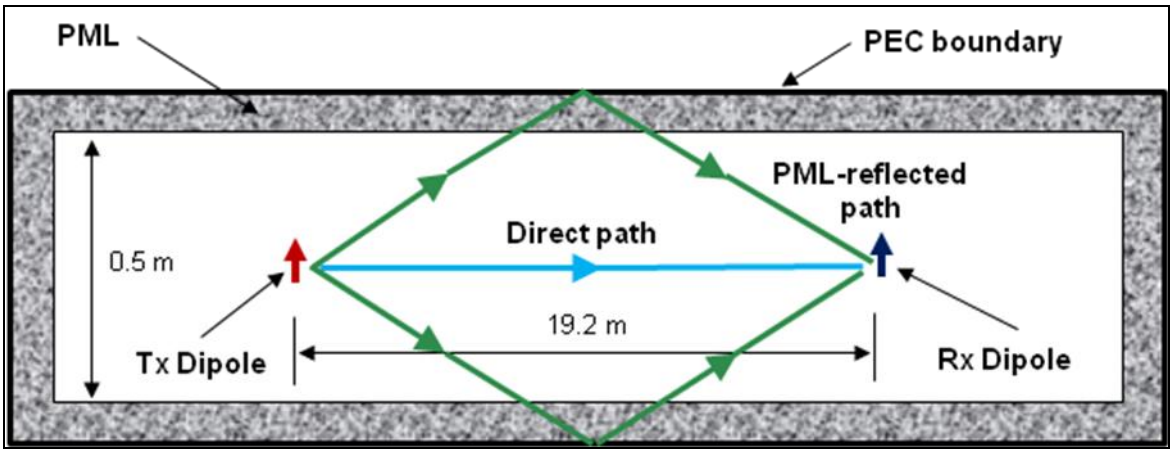

Figure 21. Schematic representation of the geometry for the example illustrating the effect of PML reflections for computational domains with large shape factors.

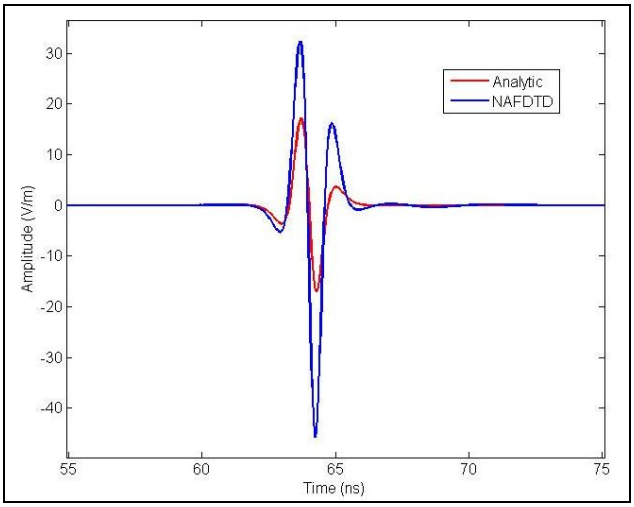

Figure 22. Comparison between the analytic and numeric time domain signals at the receiver for the example described in figure 21.

A simple prescription for mitigating this issue is to design a computational domain where the ratio of two dimensions never exceeds a certain number. Our empirical tests indicate that a maximum ratio of 5 ensures satisfactory results (that corresponds to reflections off the boundaries at angles that do not exceed 79°). For many practical applications (e.g., the analysis of a planar structure or a printed circuit board), this condition may lead to apparently wasteful use of computer resources. Future research and code development may produce a more efficient PML that could relax the computational domain shape factor requirement. Interestingly, for reasons that are not entirely clear at the time of this writing, we have not noticed this particular issue with the far-field FDTD code, although the PML implementation in both codes is identical.

4. Running the NAFDTD Code

4.1 General Considerations

The NAFDTD code shares many features with the AFDTD code described in (*1*). In order to run the NAFDTD program, the user starts by creating a project (e.g., *project_name*). The computational grids have identical structure with the AFDTD code – this includes the *project_name*.grid and *project_name*.param files. The input parameter file (*project_name*.input) is also required by the NAFDTD program, although many of its entries are ignored. More specifically, only the following lines in this file are taken into account:

- First line (algorithm type)
- Second line (running mode: “normal”, “sar”, “moca”, or “list”)
- Fourth line (excitation pulse type)
- Fifth line (pulse center frequency in Hz)
- Eighth through tenth lines (describing the output frequencies)

All the other lines in the *project_name*.input file are ignored. The entries that are not ignored should follow exactly the same rules as for the AFDTD code (*1*).

If the NAFDTD code is launched at the command prompt, the command line is the following:

nafdtd *project_name*

(Note: A second command line argument is required for running the code in SAR mode, as described in section 4.4).

The major difference between the two codes is the way the sources and receivers are specified. For the AFDTD program, the parameters describing the excitation and observation geometries are the incidence and scattering angles, which are included in the *project_name*.input file. In the

NAFDTD case, the source and receiver locations must be described as sets of coordinates of the sample points for the dipole currents (for sources) or the field probes (for receivers). These coordinates are placed in two ASCII files called *project_name*.sources (for sources) and *project_name*.savenear (for receivers). Additionally, the dipole current variation with frequency for each sample point in the source must be specified in a separate input file called *project_name*.currents. A utility program called SOURCERECEIVER (described in section 5) is provided in order to generate these three source/receiver description files.

The NAFDTD code output consists of the electric and magnetic field components at the receiver sample points. The output field values are organized in two separate files: *project_name*.tnear for time domain data and *project_name*.fnear for frequency domain data.

As with the AFDTD software, there are both serial (single core) and parallel (multiple cores) versions of the NAFDTD code. The parallel version, designed for general distributed memory systems, uses the MPI library and has a scalability characteristic similar to the AFDTD counterpart (*1*). The code has been tested on various platforms, including desktop personal computers (PCs) running the Windows 7 operating system (OS), as well as HPC platforms at Defense Supercomputing Resource Centers (DSRCs) running UNIX/Linux, such as Harold (*19*) and Raptor (*20*). There are slight differences in compiling the code on various platforms, but the general guidelines are identical to those for the AFDTD code. Since the publication of reference 1, the vast majority of computational platforms have switched to 64-bit OSs; consequently, only the 64-bit versions of the AFDTD and NAFDTD binary/executable codes will be available in the future.

The considerations related to the memory and central processing unit (CPU) time required by the NAFDTD software are again similar to those for AFDTD. A conservative prescription of allocating about 1 GB of random access memory (RAM) for 10 million cells in the grid could be applied to NAFDTD as well. Notice that, unlike AFDTD, the NAFDTD code does not need to allocate very large amounts of memory to store the incident field at all time steps during a simulation. As such, the overall memory requirements of NAFDTD are less stringent than those for AFDTD. However, the implementation of sources and receivers in the NAFDTD code could take significant memory resources that may be concentrated among a small number of computing nodes (because they are generally grouped in a small region of space). Therefore, the memory allocation should be conservative enough to avoid overcrowding the nodes that contain the sources and receivers.

When running the code on a DSRC system, a portable batch system (PBS) script file is required for launching the job in a queue. This is completely similar to that required by the AFDTD code and the job launching command consists of the following:

qsub *script_name*.pbs

A flowchart describing the process of running the NAFDTD software is presented in figure 23. The major differences with respect to the AFDTD software consist of creating the additional input files (by running the SOURCERECEIVER program) and the post-processing part, which is designed to work with completely different file formats.

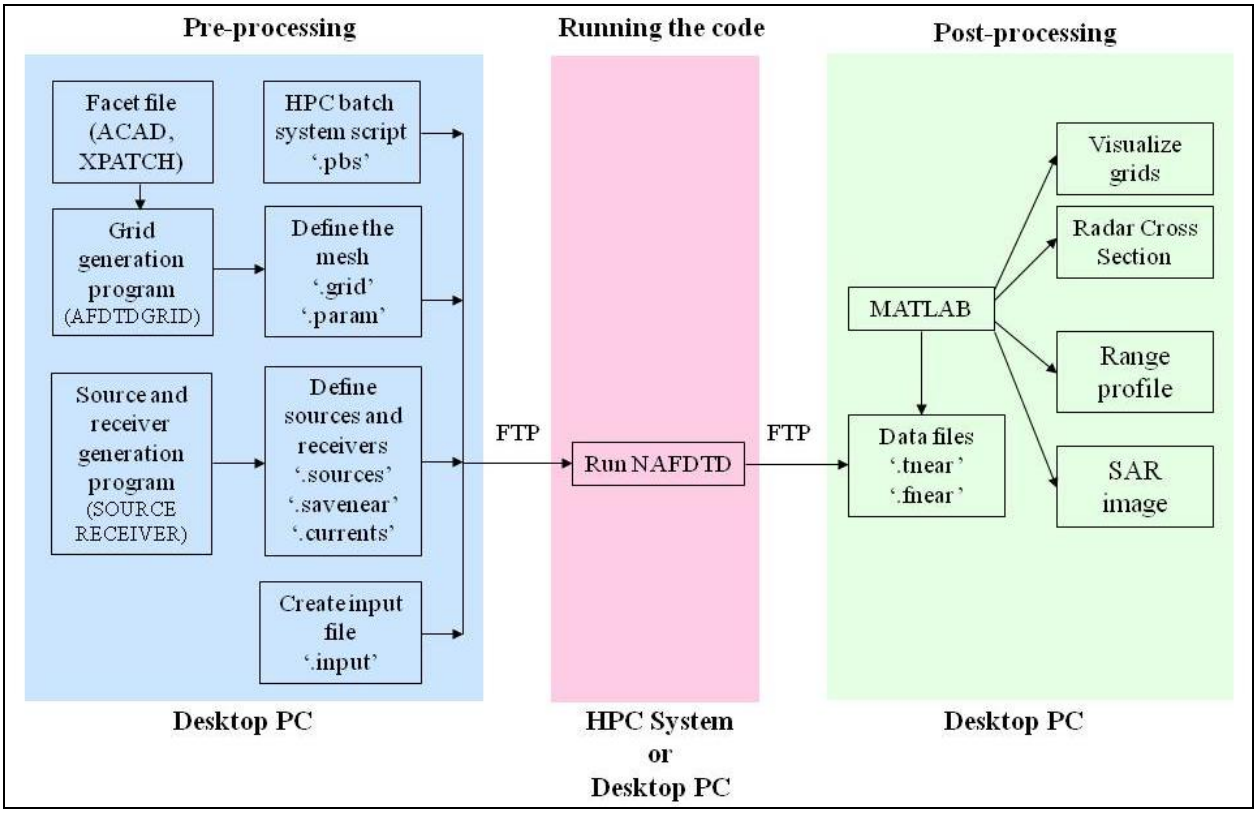

Figure 23. NAFDTD code flowchart, including pre- and post-processing.

4.2 Description of the Source and Receiver Input Files

The two ASCII files describing the spatial location of the sources and receivers for the NAFDTD program have a very similar structure. They contain the triplets of *x*, *y*, and *z* coordinates (in meters) of each sample point describing the source dipole currents and receiver field probes, respectively. They also contain information related to the number of samples in the excitation and receiver time domain sequences, as well as other general information on the simulation. Samples of the *project_name*.sources and *project_name*.savenear files are shown in figures 24 and 25.

```
scattering
direct
   4
   11
    0.500000   -0.500000   -0.025000  77
    0.500000   -0.500000   -0.020000  77
    0.500000   -0.500000   -0.015000  77
    0.500000   -0.500000   -0.010000  77
    0.500000   -0.500000   -0.005000  77
    0.500000   -0.500000    0.000000  77
    0.500000   -0.500000    0.005000  77
    0.500000   -0.500000    0.010000  77
    0.500000   -0.500000    0.015000  77
    0.500000   -0.500000    0.020000  77
    0.500000   -0.500000    0.025000  77
```

Figure 24. Example of source coordinate description file (project_name.sources).

```
  1250
  4
  -1.000000    1.000000    0.000000  77
  -1.000000   -1.000000    0.000000  77
   1.000000   -1.000000    0.000000  77
   1.000000    1.000000    0.000000  77
```

Figure 25. Example of receiver coordinate description file (project_name.savenear).

The file in figure 24 describes the locations of the current samples along a vertical wire antenna. The first line in this file indicates whether we want to simulate a radiation or a scattering problem (enter either "radiation" or "scattering" on this line). This tells the software whether the FDTD simulation is run once (for radiation) or twice (for scattering), as explained in section 3.1. The second line should read either "direct" or "huygens", depending on whether we implement the radiation sources directly as a current distribution or by means of a Huygens box (see section 2.3). As a reminder, a Huygens box can always be implemented as a collection of small dipoles (both electric and magnetic) distributed along and tangential to the surface of the box.

The radiation source currents are stored in the *project_name*.currents file (described later in this section). To reduce the file size, the stored currents can be sampled at a rate significantly lower than the temporal sampling rate of the FDTD-computed fields and later reconstructed at full sampling rate during the time-marching FDTD scheme. The third line of the *project_name*.sources file contains the down-sampling factor for the radiation source currents. The fourth line in this file represents the number of grid points where the currents are sampled to describe the radiation source (basically this number indicates how many more lines follow until one reaches the end of the file). Each of the following lines contains the triplets of *x*, *y*, and *z* coordinates (in meters) of one dipole current sample point. There is a fourth number on these lines that is ignored in the current software version.

The file in figure 25 describes the grid-point locations of four field probes acting as receivers. The first line represents the number of time domain samples that are stored in the output data files for each receiver grid point. This number is typically lower than the total number of time steps in the FDTD simulation. Notice that the output data sequences do not have to be sampled at the same rate as the excitation pulse, as long as both rates are high enough to avoid aliasing. The second line in the *project_name*.savenear file represents the number of grid points where the field probes are placed. Each of the following lines contains the triplets of *x*, *y*, and *z* coordinates (in meters) of one field probe grid point, while the fourth number on these lines is ignored in the current software version.

All the Cartesian coordinates of the sources and receivers are referenced to the physical space origin (see reference 1 for its definition in the FDTD grid). One important requirement for the dipole current sample points and the field probe grid points is that they be located inside the computational domain. If any coordinate is found outside the computational domain, the NAFDTD software displays an error message and exits. If the *x*, *y*, and *z* coordinates of one dipole current sample or a field probe do not coincide with the position of an FDTD grid point, its position is shifted to the nearest grid point. Notice that if one uses the SOURCERECEIVER program to generate the *project_name*.sources and *project_name*.savenear files, the source and receiver locations are always adjusted to coincide with FDTD grid point positions.

The *project_name*.currents file describes the dipole currents at each of the radiation source sample points. This is a binary file in single precision representation. For each source sample points (corresponding to each line in the *project_name*.sources file), we store the three electric and three magnetic current components (for a total of six components per spatial sample). In many cases, some of these components are set to zero—for instance, in the example shown in figure 24 (vertical wire antenna), only the J_z component is non-zero. As the classic description of the Yee cell suggests (*1*), the six components of the excitation currents belonging to the same FDTD cell (meaning they share the same indices *i*, *j*, *k* in equations 4 and 5) are not exactly collocated, since they are aligned with the six components of the EM field (J_x with E_x, M_x with H_x, and so on). The coordinate triplets *x*, *y*, *z* in the *project_name*.sources file always refer to the middle of the cell; the real positions of the various current component are actually displaced by half a cell in one or two directions.

Furthermore, except for some very simple, artificial scenarios, the frequency response of the radiation source described in the *project_name*.currents is not constant with frequency. Therefore, the complex response for all current components at each sample point and at all frequencies in the spectrum of interest must be stored in the file. The number of frequency samples within the spectrum of interest is computed as

$$nf = \frac{nt}{2 \times skip} + 1 \tag{8}$$

where *nt* is the total number of time steps in the FDTD simulation, while *skip* is the down-sampling factor specified on the third line of the *project_name*.sources file. The frequency spacing between two samples is given by

$$\Delta f = \frac{1}{nt \times \Delta t} \tag{9}$$

where Δt is the time step in the FDTD algorithm. Notice that the radiation source frequency response is independent of the excitation pulse spectrum. The latter is introduced during the NAFDTD simulation (according to the specification on the fourth line of *project_name*.input file), by multiplying the source response with the pulse spectrum at each frequency and converting the result to the time domain.

In summary, the *project_name*.currents file is structured as following:

- For each grid point coordinate line in the *project_name*.sources file there are six current components of the source (in order: J_x, J_y, J_z, M_x, M_y, M_z).
- For each current component there are *nf* complex numbers (in real-part/imaginary-part format) describing the frequency response of the source.
- The complex numbers are stored within three nested loops, with the frequency index varying first, the current component type varying next, and the grid point index varying last.

4.3 Description of the Output Files

The field components at the receiving grid points are saved in two separate binary files, in the time domain (*project_name*.tnear) and the frequency domain (*project_name*.fnear). The specific data recorded in these files depend on the type of modeling configuration as following:

- For the "radiation" option, the one-pass total field obtained with the full media configuration
- For the "scattering" option, the "scattered" field obtained as the difference between pass one ("total" field) and pass two ("incident" field), as explained in section 3.1

For each grid point specified in the *project_name*.savenear file, there are six field components (three electric and three magnetic) for data output. In the case of time domain data output, the field component values (real numbers) computed by the FDTD algorithm are directly saved to the output file. The number of samples in each time domain output sequence nt_{out} is given in the first line of the *project_name*.savenear file. For the frequency domain data output (complex numbers), the Fourier transform of the time-domain field components is divided by the excitation pulse spectrum, such that the result is excitation-independent. The number of frequency samples nf_{out} for this kind of output is specified on the eighth line in the *project_name*.input file.

Additional information is saved in the output files in order to facilitate data post-processing. Thus, the *project_name*.tnear file records the time ticks corresponding to the field sample sequences and the excitation pulse sequence sampled at the same rate as the field output. The *project_name*.fnear file records the frequencies of the sample points for field output.

In summary, the *project_name*.tnear file is structured as following:

- The time tick sequence (in ns) for the output data
- The excitation pulse sequence in the time domain
- For each grid point coordinate line in the *project_name*.savenear file, there are six current components of the source (in order: E_x, E_y, E_z, H_x, H_y, H_z).
- For each field component, the sequence contains nt_{out} samples (real numbers).
- The time domain samples are stored within three nested loops, with the time step index varying first, the field component type varying next and the grid point index varying last.

The *project_name*.fnear file is structured as following:

- The sequence of frequencies (in GHz) for the output data
- For each grid point coordinate line in the *project_name*.savenear file, there are six current components of the source (in order: E_x, E_y, E_z, H_x, H_y, H_z).
- For each field component, the sequence contains nf_{out} samples (complex numbers in real-part/imaginary-part format).
- The frequency domain samples are stored within three nested loops, with the frequency index varying first, the field component type varying next, and the grid point index varying last.

4.4 Running the NAFDTD Program in the SAR Mode

A primary motivation for our radar signature modeling work at ARL is to study the performance of UWB SAR systems. As mentioned in reference 1, the FDTD method in general is ideal for simulating UWB radar signature, since it can compute the target response over a wide frequency band in one time-marching run. Additionally, the AFDTD and NAFDTD codes are specifically designed to streamline the calculations required by SAR configurations. In most cases, this kind of calculations uses the job array facility available on the HPC DSRC systems via PBS batch job submission.

Running the NAFDTD program in the SAR mode is similar to running AFDTD in the same mode. The entry on the second line in the *project_name*.input file must be “sar”, while the PBS job submission script must launch a job array with as many components as different radar positions in the SAR system geometry. A sample of PBS script that submits a job array with 20

components, running the parallel NAFDTD code on the Harold system (*19*), is shown in figure 26. In this example, each component of the array uses 16 cores. Notice that the command line for the NAFDTD program includes a second argument that indicates the index of the current run in the job array.

```
#!/bin/csh
#
#PBS -k oe
#PBS -J 1-20:1
#PBS -l select=2:ncpus=8:mpiprocs=8
#PBS -l walltime=4:00:00
#PBS -N landmine
#PBS -A ARLAP01644C5C
#PBS -q challenge
#PBS -V
#
# project name: enter the AFDTD project name here
set PROJNAME = landmine
# enter the directory where the executable is placed
set EXECD = .
#
cd $PBS_O_WORKDIR
# execute the program
echo job index $PBS_ARRAY_INDEX started on `hostname` at `date`
unlimit
time mpiexec_mpt -np 16 $EXECD/nafdtd $PROJNAME $PBS_ARRAY_INDEX > $PROJNAME.log.$PBS_ARRAY_INDEX
echo job index $PBS_ARRAY_INDEX ended on `hostname` at `date`
```

Figure 26. Example of PBS job submission script for the Harold system running the NAFDTD code in the SAR mode.

Unlike in the AFDTD (far-field) code, where different radar positions meant different incidence and observation angles, in the NAFDTD (near-field) code, the radar Cartesian coordinates (specified in the *project_name*.sources and *project_name*.savenear files) are moved along the synthetic aperture track. If the "sar" mode is specified in the *project_name*.input file, then the source and receiver coordinates are interpreted differently than described in section 4.2.

An example of strip-map SAR geometry modeled with the NAFDTD program is shown in figure 27. The transmitting and receiving antennas are vertical wires of different lengths (3 cells long for the transmitting antenna and 6 cells long for the receiving antenna), offset by 2 cm in the *y* direction with respect to one another. There are 20 radar positions along the synthetic aperture (parallel to the *x*-axis), with 10 cm between two successive positions.

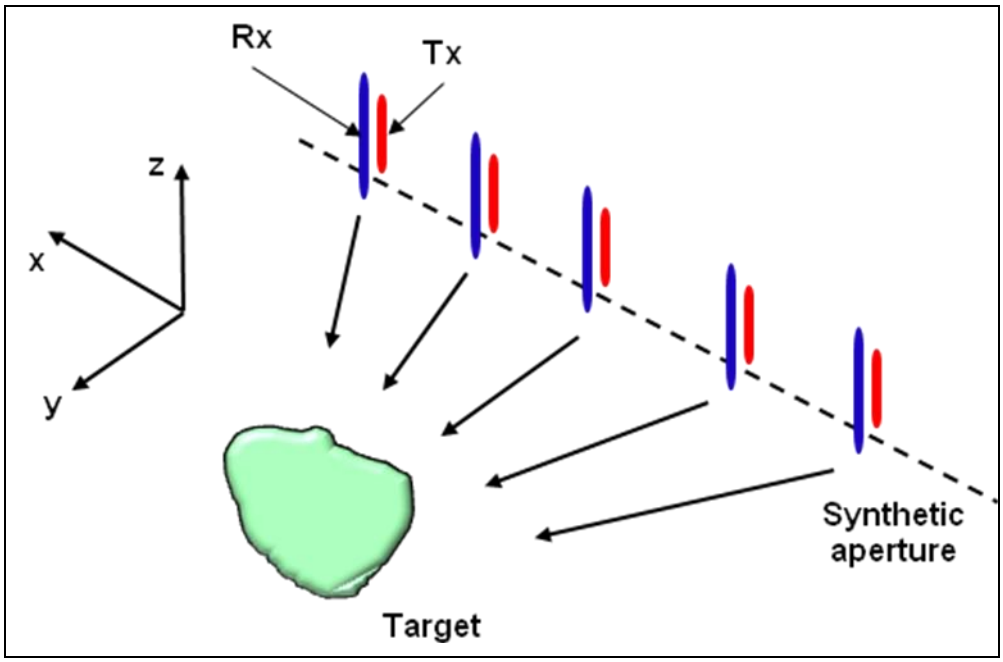

Figure 27. Schematic representation of the SAR geometry for the example in this section.

The *project_name*.sources and *project_name*.savenear files for this simulation are presented in figures 28 and 29. In the *project_name*.sources file, the fourth line indicates in this case the number of current sample grid points that make up the radiating source for one transmitting antenna position. There are three grid points describing the source for each position, and a total of $20 \times 3 = 60$ lines containing all the *x*, *y*, *z* coordinate triplets of the current samples for all transmitting antenna positions. Similarly, the second line in the *project_name*.savenear file indicates the number of field probe grid points that make up the receiver for one of its along-track positions. In this case, there are six grid points describing the receiver for each position, for a total of $20 \times 6 = 120$ lines containing all the *x*, *y*, *z* coordinate triplets of the field probes for all receiving antenna positions.

```
scattering
direct
   4
   3
   -0.500000    0.000000    0.195000  77
   -0.500000    0.000000    0.200000  77
   -0.500000    0.000000    0.205000  77
   -0.400000    0.000000    0.195000  77
   -0.400000    0.000000    0.200000  77
   -0.400000    0.000000    0.205000  77
   -0.300000    0.000000    0.195000  77
   -0.300000    0.000000    0.200000  77
   -0.300000    0.000000    0.205000  77
   -0.200000    0.000000    0.195000  77
   -0.200000    0.000000    0.200000  77
   -0.200000    0.000000    0.205000  77
   -0.100000    0.000000    0.195000  77
   -0.100000    0.000000    0.200000  77
   -0.100000    0.000000    0.205000  77
    0.000000    0.000000    0.195000  77
    0.000000    0.000000    0.200000  77
    0.000000    0.000000    0.205000  77
    0.100000    0.000000    0.195000  77
    0.100000    0.000000    0.200000  77
    0.100000    0.000000    0.205000  77
    0.200000    0.000000    0.195000  77
    0.200000    0.000000    0.200000  77
    0.200000    0.000000    0.205000  77
    0.300000    0.000000    0.195000  77
    0.300000    0.000000    0.200000  77
    0.300000    0.000000    0.205000  77
    0.400000    0.000000    0.195000  77
    0.400000    0.000000    0.200000  77
    0.400000    0.000000    0.205000  77
    0.500000    0.000000    0.195000  77
    0.500000    0.000000    0.200000  77
    0.500000    0.000000    0.205000  77
    0.600000    0.000000    0.195000  77
    0.600000    0.000000    0.200000  77
    0.600000    0.000000    0.205000  77
    0.700000    0.000000    0.195000  77
    0.700000    0.000000    0.200000  77
    0.700000    0.000000    0.205000  77
    0.800000    0.000000    0.195000  77
```

Figure 28. Partial listing of the source coordinate description file for the NAFDTD code in the SAR mode.

```
1250
6
-0.500000    0.020000    0.010000  77
-0.500000    0.020000    0.015000  77
-0.500000    0.020000    0.020000  77
-0.500000    0.020000    0.025000  77
-0.500000    0.020000    0.030000  77
-0.500000    0.020000    0.035000  77
-0.400000    0.020000    0.010000  77
-0.400000    0.020000    0.015000  77
-0.400000    0.020000    0.020000  77
-0.400000    0.020000    0.025000  77
-0.400000    0.020000    0.030000  77
-0.400000    0.020000    0.035000  77
-0.300000    0.020000    0.010000  77
-0.300000    0.020000    0.015000  77
-0.300000    0.020000    0.020000  77
-0.300000    0.020000    0.025000  77
-0.300000    0.020000    0.030000  77
-0.300000    0.020000    0.035000  77
-0.200000    0.020000    0.010000  77
-0.200000    0.020000    0.015000  77
-0.200000    0.020000    0.020000  77
-0.200000    0.020000    0.025000  77
-0.200000    0.020000    0.030000  77
-0.200000    0.020000    0.035000  77
-0.100000    0.020000    0.010000  77
-0.100000    0.020000    0.015000  77
-0.100000    0.020000    0.020000  77
-0.100000    0.020000    0.025000  77
-0.100000    0.020000    0.030000  77
-0.100000    0.020000    0.035000  77
 0.000000    0.020000    0.010000  77
 0.000000    0.020000    0.015000  77
 0.000000    0.020000    0.020000  77
 0.000000    0.020000    0.025000  77
 0.000000    0.020000    0.030000  77
 0.000000    0.020000    0.035000  77
 0.100000    0.020000    0.010000  77
 0.100000    0.020000    0.015000  77
 0.100000    0.020000    0.020000  77
 0.100000    0.020000    0.025000  77
 0.100000    0.020000    0.030000  77
 0.100000    0.020000    0.035000  77
```

Figure 29. Partial listing of the receiver coordinate description file for the NAFDTD code in the SAR mode.

In the SAR mode, the same pulse is transmitted from identical antennas for all radar positions, meaning that only one *project_name*.currents file is required to describe the excitation currents for the entire simulation. However, the data in the output files will depend on the position along the synthetic aperture. Therefore, the three digits containing the along-track index of the radar

position are appended to the output file names (e.g., *project_name*009.tnear and *project_name*009.fnear for the 9th position along the aperture), similarly to the AFDTD code.

The Monte Carlo mode, described in reference 1 for AFDTD, is also available for the NAFDTD program. However, since this mode involves multiple runs where only the grid files vary from run to run, no specific changes are required for the NAFDTD code as compared to AFDTD in this case.

5. Generating the Sources and Receivers

This section describes the utility software called SOURCERECEIVER that generates the three source and receiver input files (described in section 4.2) as a pre-processing step in running the NAFDTD program. This is an interactive command line program that is launched with the simple command **sourcereceiver**. Before starting the program, the user must make sure that the *project_name*.input and *project_name*.param files (related to the current project) are placed in the current running directory. If any of these files are missing, the program will display an error message and exit.

The interaction between the software and the user can be easily described by looking at the program screen output shown in figure 30. In this example, we assume that the NAFDTD code will run in "normal" mode (second line in the input file). The first thing the user is asked to enter is the project name (in this example, we call that "landmine"). Next, the user specifies whether NAFDTD will simulate a radiation or a scattering problem (in our case we choose "scattering"). Next entry is the down-sampling factor—for the current version of the software, this applies to both input and output time domain sequences, which will have the same number of samples. Notice that the program indicates the largest allowed value for the down-sampling factor, which does not lead to aliasing.

In the next step, the user is asked to choose between sources created from analytic expressions and sources created from numerical calculations (in this case, by FEKO simulations). In the current version of the SOURCERECEIVER software, only the first option is implemented. In that case, the radiation sources are directly introduced as dipole current samples at specific grid point. In future versions, the software will allow creating arbitrary radiation sources via a Huygens box approach, based on numeric models of antennas. It is expected that output data from the antenna modeling process will be in a ready-to-use format, such that minimal further input from the user will be required in specifying the sources.

```
 Enter the project name:
landmine

 Enter the type of electromagnetic problem:
 1. Radiation
 2. Scattering
2

 Enter the time downsampling factor (no larger than   29 )
4

 Enter a way to specify the sources:
 1. From analytic expressions
 2. From FEKO models
1

 Enter the type of source:
 1. Infinitezimal dipole
 2. Linear wire antenna
 3. Uniform rectangular aperture
 4. TE10 rectangular aperture
4

 Choose between the following options:
 1. Aperture backed by infinite PEC plane
 2. Aperture in free space
2

 Enter the aperture dimensions (in m)
 Vertical dimension = 0.1
 Horizontal dimension = 0.2

 Enter the coordinates in the center of the aperture (in m)
 x = 0
 y = 0
 z = 0

 The default aperture orientation is vertical, in the y-z plane
 Would you like to rotate the aperture? [y/n]: n

 Enter the type of receivers:
 1. Point receivers
 2. Equivalent surface receiver
1

 Enter the number of receiver points:
2

 Enter the coordinates of the receiver number   1  (in m)
 x = 2
 y = 0.2
 z = 0.2

 Enter the coordinates of the receiver number   2  (in m)
 x = 3
 y = 0.1
 z = 0.1
```

Figure 30. Screen output of the SOURCERECEIVER program with NAFDTD running in the "normal" mode.

The SOURCERECEIVER program allows four canonical types of radiation sources: infinitesimal electric current dipole, linear wire antenna, uniform rectangular aperture, and rectangular aperture of an open waveguide supporting the transversal electric $(TE)_{10}$ mode. Notice that what we call here an "infinitesimal"' dipole is in fact a small dipole of length Δx (one FDTD cell). It should also be mentioned that, except for the infinitesimal dipole, all the other

analytic current distributions created by the SOURCERECEIVER program are only approximations of the currents (or equivalent currents) that characterize the physical antennas with those structures. However, they were included in the implementation because of their mathematical simplicity and the fact that they are representative for a wide category of radar antennas.

In the example shown in figure 30, the choice is for a rectangular aperture of an open waveguide supporting the TE_{10} mode (*21*). The aperture can be backed by a PEC plane (only magnetic non-zero currents are present on the aperture) or placed in free-space (both electric and magnetic non-zero currents are present on the aperture). Since the default aperture orientation is in the *y*-*z* plane, the equivalent surface current densities are given by (assuming free-space choice and vertical polarization):

$$\mathbf{J} = -\frac{A}{Z_0}\cos\frac{\pi(y - y_0)}{a}\mathbf{z} \tag{10}$$

$$\mathbf{M} = A\cos\frac{\pi(y - y_0)}{a}\mathbf{y} \tag{11}$$

where A is a normalization constant (more on that later in this section), a is the largest of the two cross-sectional dimensions of the waveguide, y_0 is the coordinate in the middle of the aperture, Z_0 is the free-space impedance, and **y** and **z** are unit vectors. The expressions in equations 10 and 11 were obtained by applying certain approximations in conjunction with the equivalence principle (*21*) and do not represent the exact equivalent current densities on the aperture of an open rectangular guide (these can only be obtained via a numerical simulation).

Other parameters for this choice of radiating source are the aperture dimensions and position in the Cartesian space and the angle and axis of rotation with respect to the default orientation (only rotation around one axis is allowed).

If the choice were for a uniform rectangular aperture, the options for various parameters would be exactly the same, except that the surface current densities would be uniform across the aperture. This type of current distribution approximates the equivalent current densities at the open end of a parallel-plate waveguide supporting the TEM mode. An extra input parameter—the antenna polarization—must be supplied by the user in this case.

For the choice of a linear wire antenna, the default orientation is vertical and the approximate expression of the electric current along the wire is (*21*) the following:

$$\mathbf{I} = A\sin\left(k_0\left(\frac{l}{2} - |z - z_0|\right)\right)\mathbf{z} \tag{12}$$

where k_0 is the free-space propagation constant, l is the wire length, and z_0 is the coordinate of its middle (the feed point is assumed to be the middle of the wire). In the case of an infinitesimal

dipole, the length is assumed to be one FDTD cell and the current is distributed only across one cell. Both the infinitesimal dipole and the linear wire are assigned no thickness. The other parameters required by the SOURCERECEIVER program in these cases are self-explanatory.

After the radiation sources were defined, the user must define the receiver parameters. The SOURCERECEIVER software offers two receiver options: field probes at specific grid points or equivalent surface (Huygens box) receiver. Only the first option is implemented in the current software version; adding the second option is planned for future versions. Specifying the receivers simply consists of entering the number of grid points where the field probes are placed, followed by the sets of Cartesian coordinates of each grid point.

Running the SOURCERECEIVER program when the "sar" mode is chosen for the NAFDTD simulation is slightly different than in the "normal" mode. An example of program screen output for the SAR mode is shown in figure 31. Notice the message related to the fact that the NAFDTD program will run in the SAR mode. It explains that the radar is assumed to move on a linear track along one of the Cartesian axes, with the antennas placed at regular intervals along that track.

Most of the following user entries are identical to the "normal" mode. One difference is that, instead of providing the absolute coordinates of the radiating antenna (or its center), the user is asked to enter the coordinates of the first position along the track. The other parameters required are the synthetic aperture track direction, the interval between two antenna positions, and the number of positions along the aperture. The receiver antenna(s) is assumed to move similarly along the synthetic aperture, meaning that the same direction, intervals, and number of positions are used as for the radiating antenna. Consequently, only the coordinates of the first position along the aperture are required for the receiver grid points.

It is also important to be more specific about the normalization constants involved in setting the magnitude of currents for direct source implementation by the SOURCERECEIVER program. As mentioned in section 2.3, the elementary sources are always interpreted by the NAFDTD code as small electric or magnetic dipoles of length Δx with a given electric current or magnetic moment. If the user chooses an infinitesimal electric current dipole as the radiation source, its magnitude is set to 1. If the choice is for a linear wire antenna, the constant A in equation 12 is set to Δx (such that the left hand side has the dimension of an electric current moment). If the sources are represented by an aperture (uniform or TE_{10} rectangular waveguide mode), the constant A in equations 10 and 11 is set to Δx^2 (in the case of infinite PEC ground plane only the M currents are non-zero).

```
 Enter the project name:
landmine

 According to the input file, you chose the SAR mode
 The radar is assumed to move along a linear track
 The linear track must be along the x, y or z direction
 with transmit antenna positions at regular intervals
 The receivers follow a similar track as the transmitters
 (same direction and same intervals)


 Enter the type of electromagnetic problem:
 1. Radiation
 2. Scattering
2

 Enter the time downsampling factor (no larger than   29 )
4

 Enter a way to specify the sources:
 1. From analytic expressions
 2. From FEKO models
1

 Enter the type of source:
 1. Infinitezimal dipole
 2. Linear wire antenna
 3. Uniform rectangular aperture
 4. TE10 rectangular aperture
1

 Enter the dipole coordinates of the first position along track (in m)
 Maximum absolute coordinate must be less than 1000 m
 x = -0.5
 y = 0
 z = 0.2

 The default dipole orientation is vertical
 Would you like to rotate the dipole? [y/n]: y
 Dipole rotation: only rotation around one axis is allowed
 Only rotation angles less than 90 degrees are allowed
 Enter the rotation axis [x/y/z]: x
 Enter the rotation angle (degrees): 90

 Enter the SAR track direction [x/y/z]: x

 Enter the interval between two positions along track
 (negative intervals are allowed):
0.05

 Enter the number of along track positions:
20

 Enter the type of receivers:
 1. Point receivers
 2. Equivalent surface receiver
1

 Enter the number of receiver points:
1

 Enter the coordinates of the receiver number   1  (in m)
 x = -0.48
 y = 0
 z = 0.2
```

Figure 31. Screen output of the SOURCERECEIVER program with NAFDTD running in the SAR mode.

6. Code Validation and Examples

6.1 Radiation Problems Modeled by NAFDTD

In this section, we present simulations of a few radiation problems by the NAFDTD software. By studying a few canonical problems where analytic solutions are available, we can verify the accuracy of the near-field FDTD code, as well as the accuracy in implementing certain source distributions. With respect to the latter issue, we are interested in assessing the code accuracy for sources that do not conform to the FDTD Cartesian grid. All the examples shown in this section are for free-space propagation (notice that an example involving half-space propagation was presented in section 3.2, where the NAFDTD results were compared to those obtained by FEKO). The analytic solution is based on the EM field components produced by infinitesimal electric and magnetic dipoles. If a radiation source is composed of multiple elementary dipoles, the radiated field is obtained by coherently adding the contributions of all dipoles. The electric field produced by an infinitesimal electric dipole with electric current moment $\mathbf{I}l$ and arbitrary orientation in free-space is given by (*22*):

$$\mathbf{E}(\mathbf{r}) = \frac{-jk_0 Z_0 e^{-jk_0 r}}{4\pi r}\left[\mathbf{I}l\left(1-\frac{j}{k_0 r}-\frac{1}{k_0^2 r^2}\right)-\mathbf{u}_r\left(\mathbf{u}_r\cdot\mathbf{I}l\right)\left(1-\frac{3j}{k_0 r}-\frac{3}{k_0^2 r^2}\right)\right] \tag{13}$$

where $\mathbf{r}$ is the distance vector to the source, r its magnitude, and $\mathbf{u}_r$ its direction unit vector.

The first example is a one-cell vertical electric dipole placed in free-space. The excitation current is a 4th order Rayleigh pulse with center frequency of 300 MHz, and the FDTD cell size is 1.6 cm. The input files that describe the coordinates of the source and receiver are shown in figure 32.

```
radiation
direct
   4
   1
    0.000000    0.000000    0.000000  77
```

(a)

```
  300
  1
   0.320000    0.320000    0.320000  77
```

(b)

Figure 32. Files used in the dipole radiation problem, showing: (a) the source coordinates and (b) the receiver coordinates.

In figure 33 we show the time domain waveforms for two components of the electric field (E_x and E_z) at a distance of 0.32 m in all directions from the source (we choose the representation of the waveforms in the time domain because it offers a simultaneous comparison of both magnitude and phase in one graph). The match between the analytic and numeric NAFDTD solutions is virtually perfect.

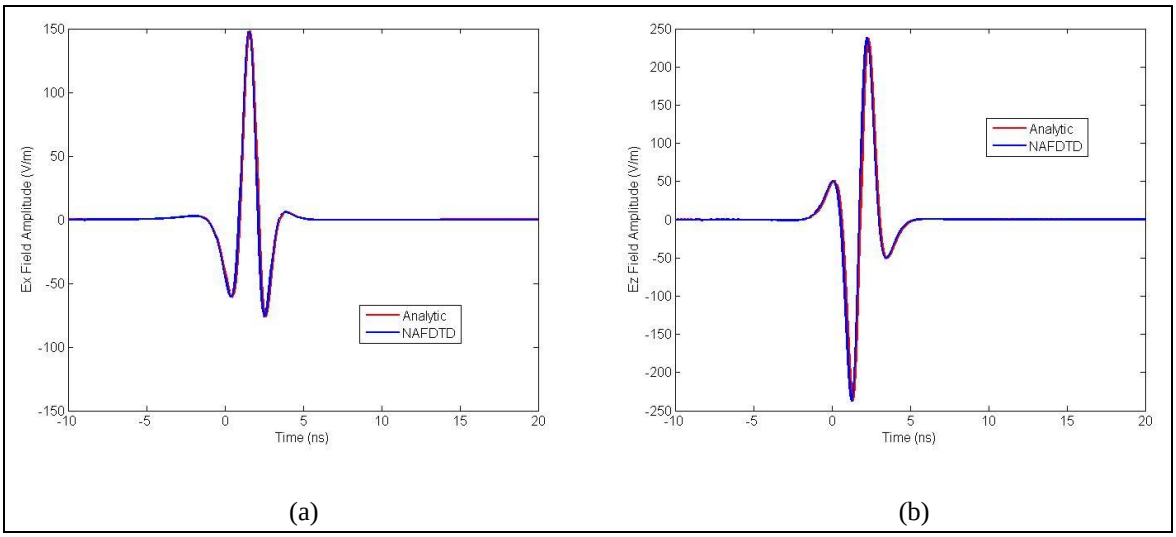

Figure 33. Comparison between the analytic and numeric NAFDTD fields radiated by a vertical dipole showing (a) E_x waveform at the receiver and (b) E_z waveform at the receiver.

A second example uses a source and a receiver at the same locations, but this time the radiating dipole has a tilt of 45° in the *x*-*z* plane. The input files describing the source and receiver coordinates are the same as those shown in figure 32; however, the structure of the "currents" file (which is binary) changes this time: both J_x and J_z are non-zero at the dipole location. The time domain waveforms for E_x and E_z at a distance of 0.32 m in all directions from the source are shown in figure 34. Again, the match between the analytic and numeric solutions is very good.

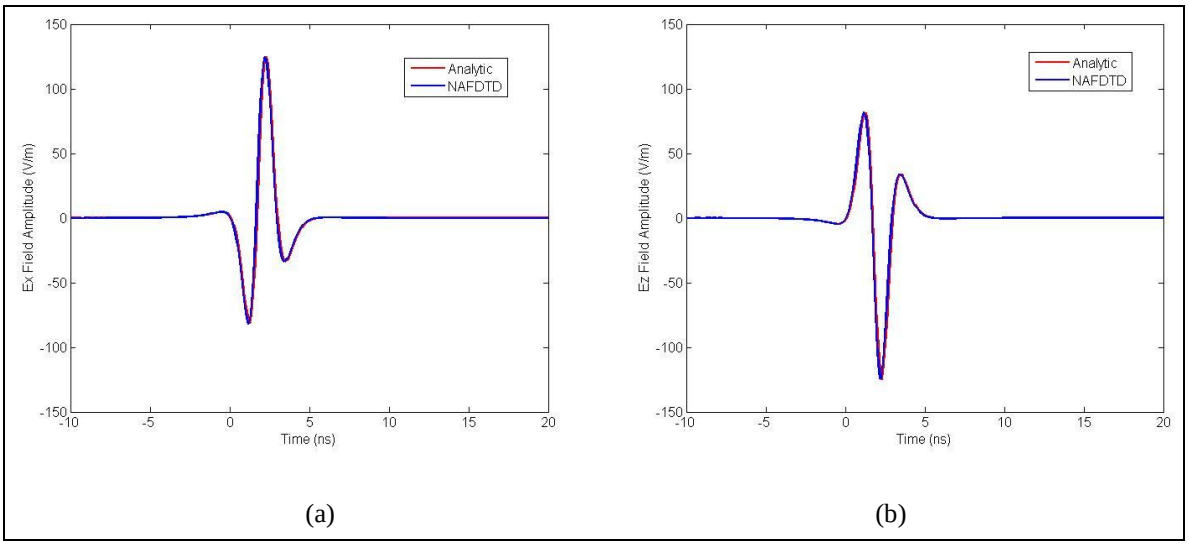

Figure 34. Comparison between the analytic and numeric NAFDTD fields radiated by an oblique dipole showing (a) E_x waveform at the receiver and (b) E_z waveform at the receiver.

The next two examples use uniform current, rectangular aperture sources. The aperture has a 0.1 m by 0.1 m size and is originally placed in free-space in vertical position (*y*-*z* plane) with vertical polarization (meaning only the J_z and M_y components of the currents are non-zero). The excitation current is again a 4th order Rayleigh pulse with center frequency of 300 MHz, while the FDTD cell size is 1 cm. The receiver is placed at 1 m in the *x* direction from the middle of the aperture. Rather than showing the source coordinate file (which is too large to fit on one page in this case), we display the screen output from running the SOURCEREIVER program for this configuration (figure 35).

We also consider a similar case, where the aperture is rotated by 20° around the *y* axis. Now we move the receiver point to correspond to the same position relative to the aperture as in the previous case (the new coordinates are 0.94, 0, and –0.24 m, respectively). The two configurations are schematically described in figure 36a. In figure 36b we show the time domain waveform for the E_z component at the receiver point obtained by three methods: analytic, numeric with the vertical aperture, and numeric with the oblique aperture (in this case, we plot $\frac{E_z}{\cos 20^{\mathbf{o}}}$). The graph demonstrates excellent agreement between the three cases.

Figure 35. Screen output of the SOURCERECEIVER program for the vertical aperture example.

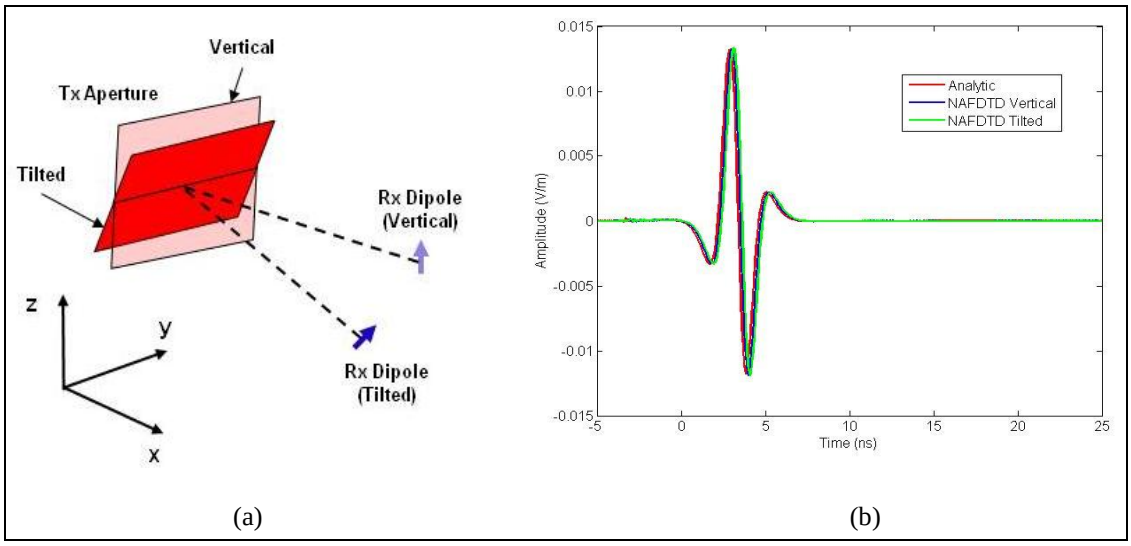

Figure 36. Comparison between the analytic and numeric NAFDTD fields radiated by rectangular aperture showing: (a) geometry of the problem and (b) time domain fields at the receiver.

6.2 Imaging of a Cylindrical Target by the NAFDTD Code

This example is more representative for the radar imaging applications of interest at ARL. The schematic configuration is shown in figure 37a. Other parameters relevant to this problem are cylinder diameter = 30 cm, cylinder height = 16 cm, ground properties $\varepsilon_r = 6$, $\sigma = 0.01$ S/m, FDTD cell size = 8 mm, and excitation by 4th order Rayleigh pulse centered at 500 MHz. The transmitter is represented by a one-cell vertical dipole at 2 m above the ground surface, placed in the middle of a horizontal 16-receiver array whose elements are spaced 12 cm with respect to one another (see figure 37b). The receiver elements are in fact field probes placed at the specific grid points. The files defining the source and receiver coordinates are shown in figure 38.

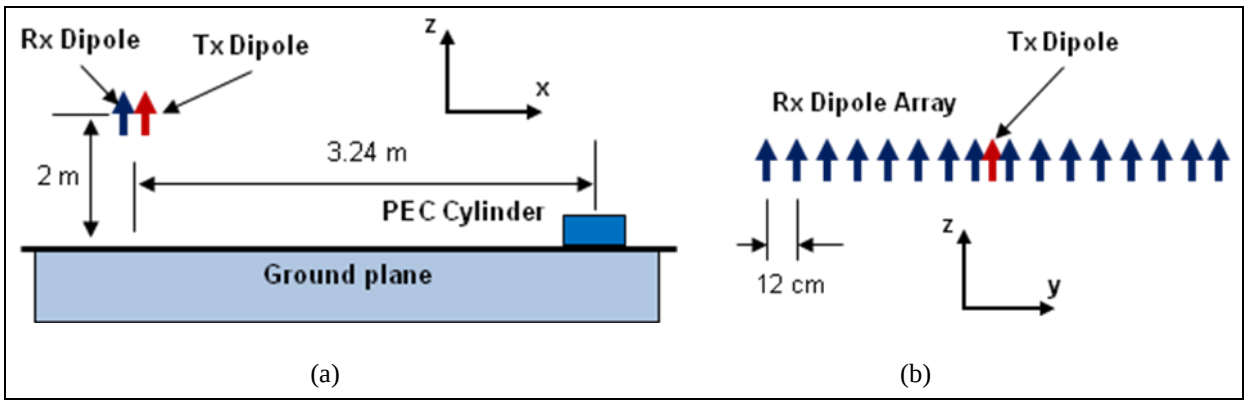

Figure 37. Schematic configuration of the radar imaging system modeled with NAFDTD showing: (a) side view of the entire geometry and (b) antenna system geometry.

```
scattering
direct
   6
   1
   0.000000  0.000000  2.00000  77
```

(a)

```
   833
   16
   0.000000 -0.900000  2.00000  77
   0.000000 -0.780000  2.00000  77
   0.000000 -0.660000  2.00000  77
   0.000000 -0.540000  2.00000  77
   0.000000 -0.420000  2.00000  77
   0.000000 -0.300000  2.00000  77
   0.000000 -0.180000  2.00000  77
   0.000000 -0.060000  2.00000  77
   0.000000  0.060000  2.00000  77
   0.000000  0.180000  2.00000  77
   0.000000  0.300000  2.00000  77
   0.000000  0.420000  2.00000  77
   0.000000  0.540000  2.00000  77
   0.000000  0.660000  2.00000  77
   0.000000  0.780000  2.00000  77
   0.000000  0.900000  2.00000  77
```

(b)

Figure 38. Files used in simulating scattering by a cylinder, showing: (a) the source coordinates and (b) the receiver coordinates.

In the first simulation, we placed the target at 3.24 m in downrange with respect to the antenna array. The scattered signals obtained at the receiver array (E_z components) are processed via a time-reversal algorithm (as described in reference 10) to obtain an image in the ground plane. The data are processed over frequency band ranging from 0.1 to 1.4 GHz. Notice that this type of image geometry does not require running the NAFDTD code in the SAR mode (since there is only one fixed transmitter position). We compared the NAFDTD results with those obtained by FEKO. Figure 39 plots the magnitude of the E_z component received at the array element placed at 0.42 m away (in the *y* direction) from the transmitter. The graphs are in agreement to within 2 dB.

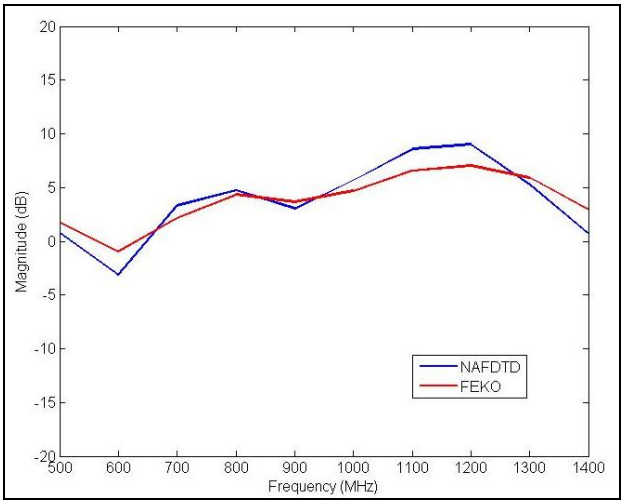

Figure 39. Comparison of the E_z magnitude vs. frequency between NAFDTD and FEKO models of cylinder scattering at near range, for a receiver point placed at 0.42 m from the transmitter.

The images obtained by the two simulation methods are shown in figure 40. Again, the agreement is very good. Notice a small artifact that appears in the NAFDTD image at about 5-m range in the *x* direction. This artifact cannot be fully explained at the time of this writing, but will be investigated and hopefully corrected in the future.

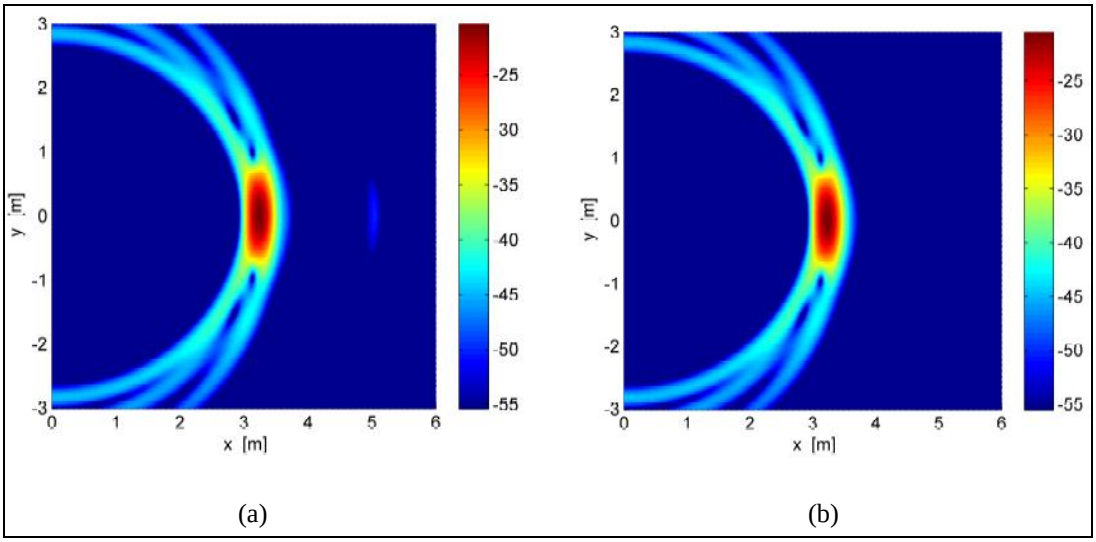

Figure 40. Images obtained for the configuration in figure 37 based on the (a) NAFDTD and (b) FEKO data.

We also performed a similar study, only this time with the target places at 18.24 m in downrange with respect to the antenna array. While for the smaller range simulation we needed only 4 cores to run the parallel NAFDTD code, the large range simulation is run on 128 cores. The PBS job submission script for the Raptor system is shown in figure 41.

```
#!/bin/csh
#
#PBS -k oe
#PBS -l ncpus=128
#PBS -l walltime=4:00:00
#PBS -N dipole
#PBS -A WPHARLAP01644C5C
#PBS -q standard
#PBS -V
#
# project name: enter the NAFDTD project name here
set PROJNAME = dipole
# enter the directory where the executable is placed
set EXECD = .
#
cd $PBS_O_WORKDIR
# execute the program
echo job started on `hostname` at `date`
time aprun -n 128 $EXECD/nafdtd $PROJNAME > $PROJNAME.log
echo job ended on `hostname` at `date`
```

Figure 41. PBS job submission script for the Raptor system for the far-range cylinder imaging example.

The comparison between NAFDTD and FEKO results for the long-range simulation is shown in figures 42 (magnitude of E_z at 0.42 m from the transmitter) and 43 (in the image domain). A similar comment regarding the NAFDTD image artifact applies as in figure 40.

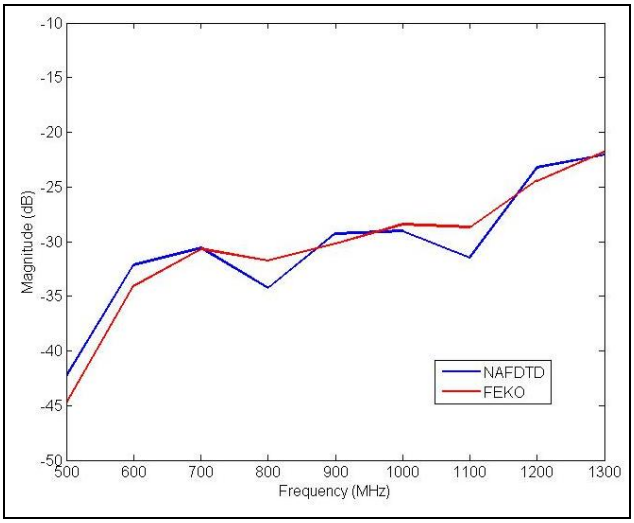

Figure 42. Comparison of the E_z magnitude vs. frequency between NAFDTD and FEKO models of cylinder scattering at far range, for a receiver point placed at 0.42 m from the transmitter.

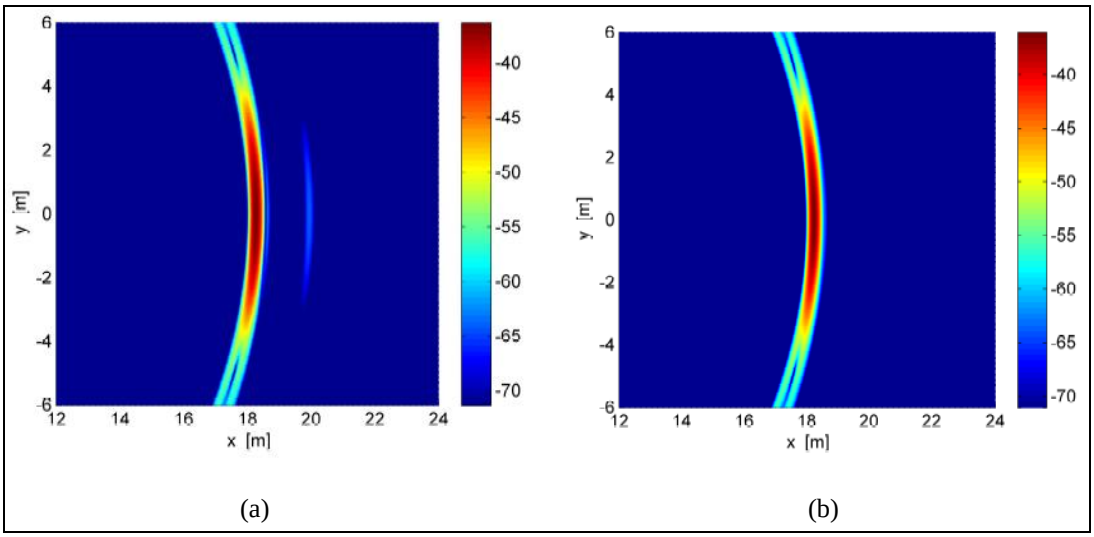

Figure 43. Images obtained for the cylinder at far range based on the (a) NAFDTD and (b) FEKO data.

Notice the differences between the images in figures 40 and 43, which were already mentioned in section 2.4. Thus, the target at the larger range appears less localized (poorer cross-range resolution) and its sidelobes have different curvature. These effects are caused by the fact that the imaging integration angle becomes smaller for a fixed-size aperture placed at a larger distance. Additionally, the target brightness in the images in figure 43 is lower than in figure 40—this can be attributed to the closer-to-grazing aspect angle of the far-range target, which significantly reduces the radar return of the target in the presence of a ground plane.

7. Conclusions and Future Work

In this report we have described the near-field FDTD code developed at ARL. After providing a motivation for having such a modeling tool alongside with the far-field FDTD code and discussing implementation issues specific to the near-field code, we created a user's guide to running the software. Finally, we presented some examples that provided validation for the code.

For the future, we envision the NAFDTD software to become a major asset in the ARL suite of EM simulation tools applied to radar problems. Arguably, the NAFDTD code may provide a more accurate and realistic solution to many Army radar scenarios than the AFDTD far-field code.

A major hurdle for the NAFDTD code is the fact that it requires interfacing with other software in order to model the antenna input and output. One obvious candidate for pre- and post-processing antenna data is FEKO. Work is currently underway to develop software interfaces between the two programs. Another issue is that, compared to the AFDTD software, NAFDTD may require additional resources to model a similar size problem in order to accommodate the

radar transmitter and receiver. However, given the ever-expanding computing power of the DSRC centers, this should not constitute a serious obstacle in the long run.

Finally, the near- and far-field FDTD codes should be merged into one single software package. This should be facilitated by the fact that the two codes share many of the input files, particularly the grid description files. Generally, the near-field scenario would require additional input information related to the source and receiver configuration. At the same time, the output should be provided both in the near- and far-field zones at the user's request. This means that, in addition to the current separate configurations, one should be able to output near-field data for far-field excitation or far-field data for near-field excitation. Such feature would greatly enhance the flexibility and applicability of the simulation software.

8. References

1. Dogaru, T. *AFDTD User's Manual*; ARL-TR-5145; U.S. Army Research Laboratory: Adelphi, MD, March 2010.
2. Balanis, C. *Advanced Engineering Electromagnetics*; Wiley: New York, 1989.
3. Taflove, A.; Hagness, S. *Computational Electrodynamics: The Finite-Difference Time-Domain Method*, Artech: Norwood, MA, 2000.
4. FEKO EM Simulation Software Web page. http://www.feko.info (accessed October 2011).
5. Dogaru, T.; Le, C.; Nguyen, L. *Synthetic Aperture Radar Images of a Simple Room Based on Computer Models*; ARL-TR-5193; U.S. Army Research Laboratory: Adelphi, MD, May 2010.
6. Dogaru, T.; Le, C.; Nguyen, L. *Through the Wall Radar Simulations for Complex Room Imaging*; ARL-TR-5205; U.S. Army Research Laboratory: Adelphi, MD, May 2010.
7. Liao, D. *Full-wave Characterization of Rough Terrain Surface Effects for Forward-looking Radar Applications: A Scattering and Imaging Study from the Electromagnetic Perspective*; ARL-TR-5758; U.S. Army Research Laboratory: Adelphi, MD, Sep. 2011.
8. Soumekh, M. *Synthetic Aperture Radar Signal Processing*; Wiley: New York, 1999.
9. Ressler, M.; Nguyen, L.; Koenig, F.; Wong, D.; Smith, G. The ARL Synchronous Impulse Reconstruction (SIRE) Forward-Looking Radar. *Proc. SPIE* **May 2007**, *6561*.
10. Liao, D.; Dogaru, T.; Sullivan, A. Emulation of Forward-Looking Radar Technology for Threat Detection in Rough Terrain Environments: A Scattering and Imaging Study. *Proc. of HPCMO*, 2012.
11. NIITEK Web page. http://www.niitek.com (accessed May 2012).
12. Nguyen, L.; Dogaru, T.; Innocenti, R. 3-D SAR Image Formation for Underground Targets Using Ultra-Wideband (UWB) Radar. *Proc SPIE* **2009**, 7308.
13. Nguyen, L.; Dogaru, T. Detection of Underground Target Using Ultra-Wideband Borehole Radar and SAR Image Formation. *Proc. SPIE* **2006**, 6210.
14. Skolnik, M. I. *Introduction to Radar Systems*, McGraw Hill, New York, 2001.
15. Hubral P.; Tygel, M. Analysis of the Rayleigh pulse. *Geophysics* **1989**, *54*, 654–658.

16. Dogaru, T.; Le, C. *Simulated Radar Range Profiles of Simple Room as Computed by FDTD and Xpatch*; ARL-TR-4420; U.S. Army Research Laboratory: Adelphi, MD, April 2008.

17. Berenger, J. P. A Perfectly Matched Layer for the Absorption of Electromagnetic Waves. *Journal of Computational Physics* **October 1994**, *114*, 185–200.

18. Fang, J.; Wu, Z. Generalized Perfectly Matched Layer - an Extension of Berenger's Perfectly Matched Layer Boundary Condition. *IEEE Microwave and Guided Wave Letters*, **December 1995**, *5*, 451–453.

19. ARL DSRC Web page. http://www.arl.hpc.mil (accessed June 2012).

20. AFRL DSRC Web page. http://www.afrl.hpc.mil (accessed June 2012).

21. Balanis, C. *Antenna Theory – Analysis and Design*, Wiley: New York, 1997.

22. Kong, J. A. *Electromagnetic Wave Theory*; EMW Publishing: Cambridge, MA, 2000.

List of Symbols, Abbreviations, and Acronyms

3-D	three-dimensional
AFRL	U.S. Air Force Research Laboratory
ARL	U.S. Army Research Laboratory
BPA	backprojection algorithm
CEM	computational electromagnetics
CPU	central processing unit
DSRC	Defense Supercomputing Resource Center
EM	electromagnetic
FDTD	Finite Difference Time Domain
GPR	ground penetrating radar
HPC	High-Performance Computing
MPI	message passing interface
NIITEK	Non-Intrusive Inspection Technology
OS	operating system
PBS	portable batch system
PC	personal computer
PEC	perfect electric conductor
PML	perfectly matched layer
RAM	random access memory
RF	radio frequency
SAR	synthetic aperture radar
SIRE	Synchronous Impulse Reconstruction
STTW	sensing through the wall
TE	transversal electric
TEM	transversal electromagnetic
UWB	ultra-wideband

No. of Copies	Organization
1 (PDF only)	DEFENSE TECHNICAL INFORMATION CTR DTIC OCA 8725 JOHN J KINGMAN RD STE 0944 FORT BELVOIR VA 22060-6218
15	US ARMY RSRCH LAB ATTN RDRL CIO LT TECHL PUB ATTN RDRL CIO LL TECHL LIB ATTN RDRL SER M W O COBURN ATTN RDRL SER U A SULLIVAN C LE C KENYON G KIROSE D LIAO C TRAN K KAPPRA T DOGARU (4 COPIES) ATTN IMAL HRA MAIL & RECORDS MGMT ADELPHI MD 20783-1197

TOTAL: 16 (1 ELEC, 15 HCS)

INTENTIONALLY LEFT BLANK.